Developmental Biology 456 (2019) 164–178

Contents lists available at ScienceDirect

Developmental Biology

journal homepage: www.elsevier.com/locate/developmentalbiology

Original research article

Integrated K+ channel and K+Cl- cotransporter functions are required for the coordination of size and proportion during development

Jennifer S. Lanni [a,*], David Peal [b,c], Laura Ekstrom [a], Haining Chen [a], Caroline Stanclift [a], Margot E. Bowen [b,c], Adriana Mercado [d], Gerardo Gamba [e,f], Kristopher T. Kahle [g], Matthew P. Harris [b,c,**]

[a] Department of Biology, Wheaton College, Norton, MA, 02766, USA
[b] Department of Genetics, Harvard Medical School, Boston, MA, 02124, USA
[c] Department of Orthopaedic Research, Boston Children's Hospital, Boston, MA, 02124, USA
[d] Instituto Nacional de Cardiología Ignacio Chávez, Mexico
[e] Molecular Physiology Unit, Instituto de Investigaciones Biomédicas, Universidad Nacional Autónoma de México and Instituto Nacional de Ciencias Médicas y Nutrición Salvador Zubirán, Mexico
[f] Tecnológico de Monterrey, Escuela de Medicina y Ciencias de la Salud, Mexico
[g] Departments of Neurosurgery, Pediatrics, and Cellular & Molecular Physiology, and NIH-Rockefeller Center for Mendelian Genomics, Yale School of Medicine, New Haven, CT, 06511, USA

A B S T R A C T

The coordination of growth during development establishes proportionality within and among the different anatomic structures of organisms. Innate memory of this proportionality is preserved, as shown in the ability of regenerating structures to return to their original size. Although the regulation of this coordination is incompletely understood, mutant analyses of zebrafish with long-finned phenotypes have uncovered important roles for bioelectric signaling in modulating growth and size of the fins and barbs. To date, long-finned mutants identified are caused by hypermorphic mutations, leaving unresolved whether such signaling is required for normal development. We isolated a new zebrafish mutant, *schleier*, with proportional overgrowth phenotypes caused by a missense mutation and loss of function in the K^+-Cl^- cotransporter Kcc4a. Creation of dominant negative Kcc4a in wild-type fish leads to loss of growth restriction in fins and barbs, supporting a requirement for Kcc4a in regulation of proportion. Epistasis experiments suggest that Kcc4a and the two-pore potassium channel Kcnk5b both contribute to a common bioelectrical signaling response in the fin. These data suggest that an integrated bioelectric signaling pathway is required for the coordination of size and proportion during development.

1. Introduction

Anatomical systems depend on scaling properties to function such that as size increases, structure of tissues and their interactions change to accommodate (Huxley, 1932; Huxley and Teissier, 1936). In many systems this scaling is a property of morphogenetic fields and differential read out as size changes; in other contexts, scaling has been attributed to space filling models and reaction diffusion-based patterning (Othmer and Pate, 1980; Umulis and Othmer, 2013). A lasting question in scaling is how overall size is determined such that there is a relative growth of structures in relation to total body size (Vollmer et al., 2017) - in other words, how do structures know when to stop growing? These relative proportions are established in development and maintained such that they are renewed in regenerating systems. When tissues fail to coordinate these patterning functions within structures or have dysregulated overall growth, aberrant cell behavior and neoplasm often result.

Genetic analyses have been utilized to great effect over the last several decades to identify the molecules that regulate size and growth of structures during development and regeneration. Many of these genetic factors act as components of transcriptional networks functioning downstream of intercellular signaling peptides and hormones that control systemic regulation of local tissue and cell behavior. In growth regulation, genes such as *hippo/yap* and insulin growth factors have been tied to overgrowth and size regulation (reviewed in (Gokhale and Shingleton, 2015; Watt et al., 2017). However, the overarching mechanism of developmental signaling that mediates coordinated growth and relative proportion remains enigmatic.

Recently, research has revealed the importance of additional

* Corresponding author.
** Corresponding author. Department of Genetics, Harvard Medical School, Boston, MA, 02124, USA.
E-mail address: lanni_jennifer@wheatoncollege.edu (J.S. Lanni).

https://doi.org/10.1016/j.ydbio.2019.08.016
Received 9 May 2019; Received in revised form 7 August 2019; Accepted 23 August 2019
Available online 28 August 2019

pathways such as bioelectric signaling in governing growth and coordinated development within and between tissues. Bioelectric signals stemming from local cell and tissue sources as well as broader systemic sources such as electrical fields have been found to be associated with organized biological structures such as tissues, organs and organisms (Levin et al., 2017). At the cellular level, bioelectric signaling can be observed to regulate the proliferation rate of cells via alterations in transmembrane voltage gradients (V_{mem}). These changes in V_{mem} can also be transduced within tissue layers by cellular junctions to create tissue-wide bioelectric gradients that effect changes in large-scale patterning (Levin et al., 2017). Despite this progress, much remains to be elucidated about bioelectrical signaling networks, from the specific molecules that determine transmembrane voltage gradients to the mechanisms by which these gradients are expressed in body patterning and growth. Further, the informative nature of such bioelectric signals in development has been an open question for over the last 120 years of research, and it remains unclear if these signals are a consequence of, or a specific regulator of development and tissue/organ homeostasis.

Forward mutagenesis screens in zebrafish have identified several genes that are implicated in both bioelectric signaling and body patterning. The distinctive striped pigment pattern in adult zebrafish is altered by mutation of the potassium channel *kcnj13 (obelix/jaguar* (Iwashita et al., 2006),); this phenotype has been shown to be due to the absence of cell depolarization normally triggered by contact between pigment cells (Inaba et al., 2012). Similarly, mutations in the gap junction proteins encoded by *cx39.4 (luchs)* and *cx41.8 (leopard)* also affect pigment stripe width or integrity (Irion et al., 2014; Watanabe et al., 2006). Interestingly, adult fin size is also regulated by proteins with conductive properties. Mutation of the *cx43* gene causes a short fin phenotype (Iovine et al., 2005) that is proportional to loss of junctional conductance (Hoptak-Solga et al., 2007; Misu et al., 2016). We have previously identified the two-pore potassium channel *kcnk5b* as an important mediator of fin size regulation in zebrafish. Specifically, fish with activating mutations in *kcnk5b* exhibit proportional overgrowth of the fins and barbels that is wholly dependent upon channel conductivity. *Kcnk5b* expression is also required for fin overgrowth induced by inhibition of calcineurin, providing a link between bioelectric signaling and transcriptional regulation by calcineurin. The cases of enhanced growth or patterning seen in the long-finned or broad-stripe phenotypes described above are quite informative, as loss of structures can occur for many genetic and physiological reasons but enhanced growth indicates specificity of regulation. However, the chemical treatments and genetic alleles identified thus far that cause proportional fin overgrowth are all gain-of-function and may thereby reflect a supra-physiological response of tissues to novel growth enhanced conditions, whether bioelectrical or chemical.

In this work, we identify a novel zebrafish mutant, *schleier*, that affects both fin length and pigment pattern in the adult fish and is similar in fin phenotype to gain of function mutants of *kcnk5b* (Perathoner et al., 2014). We show that these phenotypes are due to inactivation of the potassium-chloride cotransporter *slc12a7a/kcc4a*, which carries out electroneutral symport across the plasma membrane. While *slc12a7* paralogues have not previously been studied in zebrafish, the orthologue of *slc12a7a* has a broad expression pattern in mammals and is linked to diverse functions in the kidney, inner ear, and gastric and prostate glands (Boettger et al., 2002) (Marcoux et al., 2017). Importantly, we demonstrate that proportional growth of zebrafish appendages encompassing fins and barbels is altered in fish with dominant negative alleles of *slc12a7a/kcc4a*, suggesting that potassium regulation establishes the normal size of these appendages in development. Further, we find that the enhanced growth effects stemming from Kcc4a mutant alleles are attenuated by *kcnk5b* inactivation, suggesting that these two channels act in a similar pathway. The *schleier* mutation in Kcc4a also disrupts normal pigment pattern in the adult fish, resembling zebrafish mutants that affect gap junction function. We also show that Kcc4 mutation in fins results in a dramatic change in fin vasculature, providing a potential mechanistic connection between vascularization, potassium regulation and fin growth.

Our work highlights the growing importance of bioelectric signaling in growth regulation and coordinated patterning of complex structures. Through our systematic mutagenesis analysis in the zebrafish, we have identified a role for bioelectric signaling in development that integrates environmental, systemic, and canonical intracellular signaling inputs.

2. Results

2.1. Identification and characterization of schleier mutant zebrafish

In a screen to identify dominant modifiers of *longfin*^{dt2} (*lof*) mutant zebrafish, a mutant was identified that showed additive effects with *lof* on fin length (Supplementary Fig. 1). This mutation segregated away from the *lof* locus and was isolated. Given the flowing fin morphology, we named this mutant *schleier (schl) (*German, "veil"). Heterozygous *schleier* mutants exhibit changes in proportion of all fins and barbels (Fig. 1B). This effect is dose dependent with homozygotes exhibiting slightly dysmorphic fins due to internal fractures of the fin rays (Fig. 1C, F). Although present in expected frequencies at juvenile stages, homozygous *schleier* mutants had decreased fitness and survival rates (data not shown). The heterozygous *schleier* mutant closely resembles fin overgrowth morphologies observed in gain-of-function mutations in the potassium channel *kcnk5b* in the mutants *another longfin (alf)* and *pfau* (Perathoner, 2014); however, the new mutation was not linked to the *kcnk5b* locus (data not shown). Heterozygous *schleier* caudal fins often contained thick, dysmorphic bone segments near the peduncle and on the ventral and dorsal margins of the fin, as well as evidence of bone breakage and healing, resulting in aberrant segments (Supplementary Fig. 2A).

In addition to the dominant fin and barbel length phenotypes, the *schleier* homozygous mutant also has a novel recessive phenotype affecting stripe formation. The pattern of pigmentation along the flank of homozygotes results in broken stripes which at times resolve into spots (Fig. 1I). Stripe pattern in the caudal and anal fins is also greatly disrupted. This phenotype is not present in *kcnk5b* mutants, which do not affect normal stripe patterning (Perathoner et al., 2014). Thus, the *schleier* mutant is a unique locus sharing many of the same phenotypes as *alf/kcnk5b* mutants but with a separate role in stripe patterning during late development.

To characterize changes in fin growth, we measured caudal fin length and standard length of *schleier* heterozygotes and wildtype siblings during post-embryonic development. *Schleier* homozygotes were not used for fin analyses as they had dysmorphic fins and fin ray segments, making them less suitable for linear comparisons (Fig. 1C, F). When compared to wild-type individuals, *schleier* heterozygotes displayed an increased rate of fin growth relative to standard length throughout development, leading to overall positive allometry ($\alpha = 1.35$) of the fins (Fig. 1J). Such alterations in fin proportion could be caused by patterning changes in the number and/or size of segments in the dermal rays. We find that *schleier* caudal fin rays show elongation of segment size while retaining similar numbers of segments as wild-type fish (Supplementary Figs. 2B and 2C); elongated fin segments were also observed in *schleier* anal fin rays (Supplementary Fig. 2D). This finding resembles the phenotype of the *another longfin (alf) or pfau* long-finned mutants, which exhibit comparable changes in fin skeletal patterning and are caused by gain of function-alterations in Kcnk5b (Perathoner et al., 2014). Given the phenotypic similarity between these mutants and that our previous work linked *alf/kcnk5b* function to bioelectric signaling in development (Daane et al., 2018), we chose to further characterize *schleier* as it might reveal mechanistic aspects of bioelectric signaling in size regulation.

2.2. Schleier mutation highlights role of vascular tone associated with altered proportionality in zebrafish fins

In addition to their overgrown fins and barbels, one notable feature of the *schleier* mutant fish is their unusual fin vasculature. Under light microscopy, caudal fins of live *schleier* fish are seen to have enlarged blood

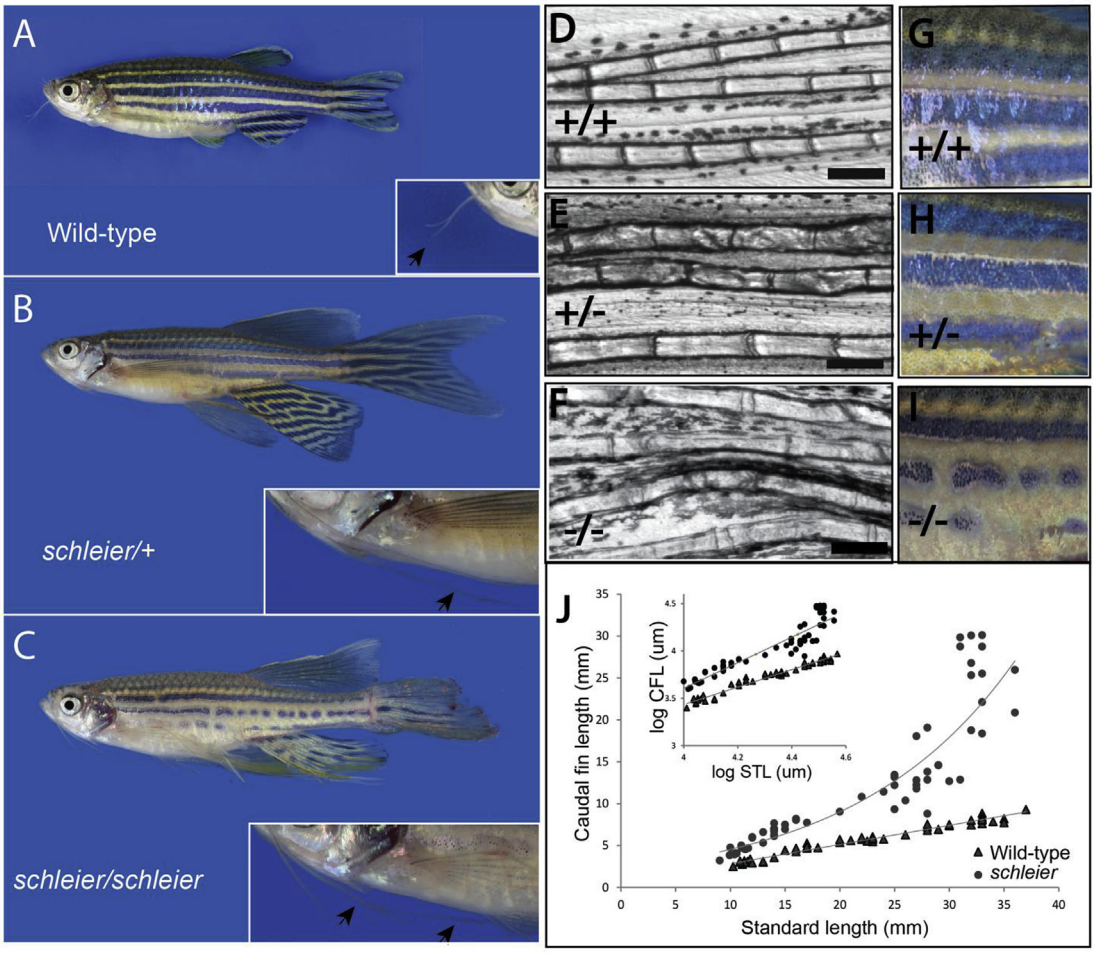

Fig. 1. Dominant enhancer of *longfin* causes increased fin proportion through enhanced relative growth of the fin during development. A, B, C) Phenotype of *schleier* mutant zebrafish affects fin and barbel proportion and pigmentation of the adult zebrafish in a dose dependent manner. **D, E, F)** Segment length of lepidotrichia from adult caudal fins of wild-type, heterozygous, and homozygous *schleier* fish. Bar represents 200 μM. **G, H, I)** Close up of pigment pattern on flank of wild-type, heterozygous, and homozygous *schleier* fish. **J)** Growth curves of caudal fin length in wild-type and *schleier* heterozygous fish as a function of standard length (STL). *Inset*, Log-log plot of caudal fin length vs. STL to illustrate allometric scaling of growth. Wild-type: $y = 0.9209x - 0.2495$, $R^2 = 0.97$. *Schleier*, $y = 1.3498x - 1.7933$, $R^2 = 0.89$.

vessels and alterations in flow rate to and from the fin tip. We characterized the vascular phenotype in more depth in wild-type and heterozygous *schleier* fins in order to identify possible mechanisms underlying fin overgrowth. We crossed the *schleier* mutation into a transgenic strain, *Tg(fli1:EGFP)*, in which green fluorescent protein is expressed in all vasculature (Lawson and Weinstein, 2002). Wild-type fish displayed the expected caudal fin vasculature extending along fin rays of one centrally located artery flanked by two veins in each fin ray (Fig. 2A, C). These primary vascular elements were connected to one another by inter-vessel commissures, and to adjoining veins by inter-ray vessels. *Schleier* heterozygous fish retained overall normal vascular patterning, with significantly enlarged diameter of blood vessels and increased number of *fli* + endothelial cells lining vessels (Fig. 2B, D). To investigate the functional consequence of these changes, we performed high-speed videomicroscopy on *fli1:eGFP* caudal fins of live wild-type and *schleier* heterozygous fish. Data were analyzed to determine the velocity of individual red blood cells in veins and arteries as well as the diameter of the corresponding veins and arteries in the tissue proximal to the fin tip. The veins of *schleier* mutant fish had a consistently larger diameter relative to the adjacent artery, resulting in an increased vein:artery diameter ratio (Fig. 2E). This structural change was accompanied by a change in the relative rates of blood flow in *schleier* vessels (Supplementary Movies 1, 2). We quantitated this phenotype by measuring the relative vein:artery velocity, and found that relative venous flow was almost twice as slow in *schleier* caudal fins as compared to wild-type fins (Fig. 2F). The result of this varied flow rate was apparent in gross inspection of the *schleier* mutant, as pooling of blood is often seen at distal tips of overgrown *schleier* fins and barbs (Fig. 2H) but not in wild-type fins (Fig. 2G).

2.3. *Schleier is caused by mutation of slc12a7a encoding potassium chloride cotransporter kcc4a*

As the *schleier* mutation originated from a screen on homozygous *lof(dt2)* background, the *schleier* locus will retain a *lof*-specific haplotype in the region of the mutation. Outcross of the original F1 mutant revealed that the mutation was linked to the *lof* locus but could be recombined away from it (39/134 outcross progeny). We then used homozygosity mapping and massively parallel sequencing (methods previously defined in (Bowen et al., 2012)) to link the *schleier* mutation to the *slc12a7a/kcc4a* gene on chromosome 2. To screen for potential causative mutations, we used whole-genome-sequencing-generated databases of variant SNPs for the *lof* background (Bowen et al., 2012) to identify unique changes that were present in *schleier* and never seen in *lof*. From this analysis, we identified two SNPs located in *slc12a7a/kcc4a* on Chromosome 2 that were unique to the *schleier* mutant sequence. One SNP was located in the 3' UTR of a putative alternative transcript, while the other SNP led to a missense mutation (C583Y) of a conserved residue in exon 14 in the primary transcript of the gene. Through outcrossing the

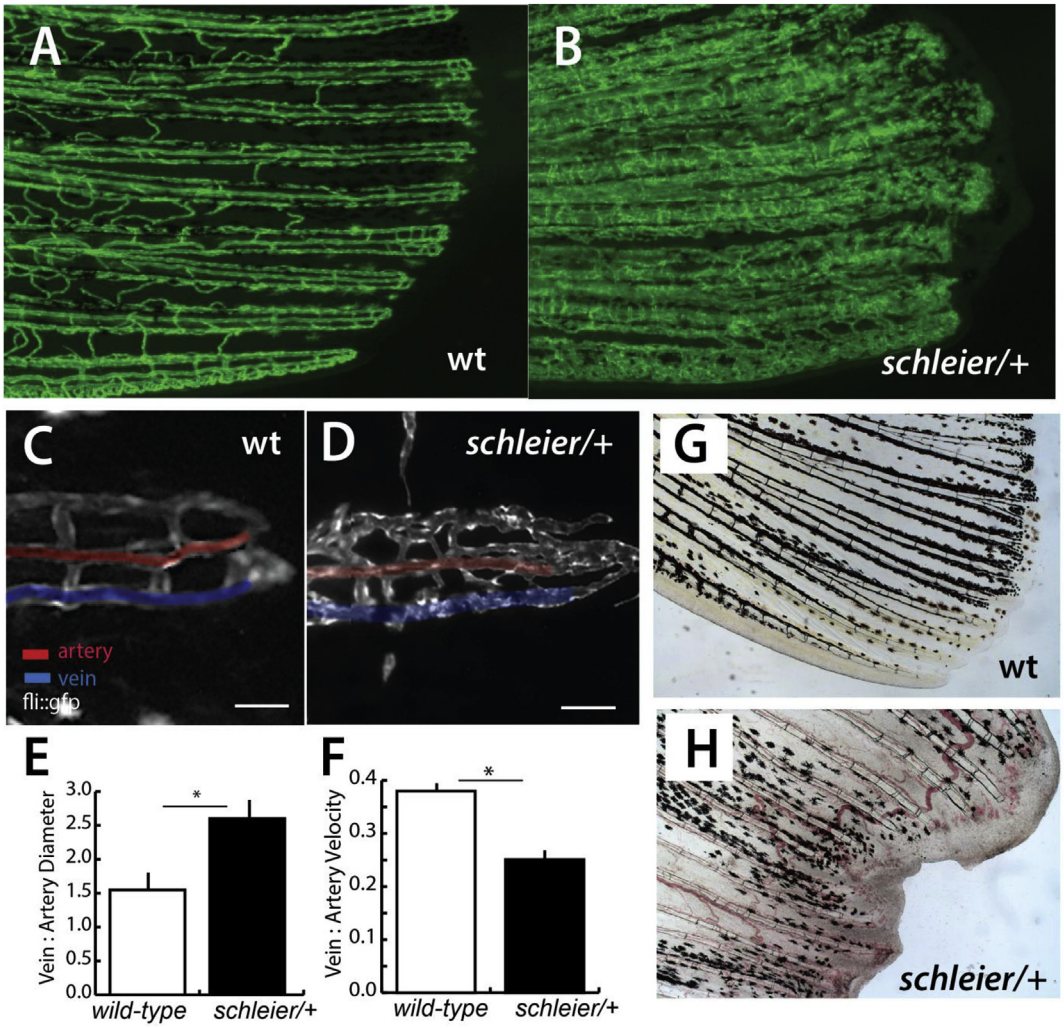

Fig. 2. ***Schleier*** **mutation highlights role of vascular tone associated with altered proportionality in zebrafish fins. A, B)** Pattern of vascularization in caudal fins of adult wild-type (wt) and *schleier* heterozygous fish visualized by *Tg(fli1:egfp)* transgenic expression of endothelial cells. **C, D**) Close up of caudal fin tip showing venous and arterial pattern variation in the *schleier* mutant associated with increased number of endothelial cells. Veins and arteries pseudo-colored blue and red, respectively; scale bar equals 100 μM. **E**) Measure of vascular dilation in *schleier* caudal fin tips. Mean ± standard error of mean (SEM) is shown. *, $p < 0.05$ by ANOVA. N = 3 fish per genotype; mean of 5 artery and 5 vein diameter measurements per fish. **F**) Quantitation of vascular flow in fin tip in arteries compared with veins. Mean ± standard error of mean (SEM) is shown *, $p < 0.05$ by ANOVA. N = 3 fish per genotype; mean of 10 arterial red blood cells and 10 venous red blood cells per fish. **G, H**) Excessive vascularization and blood pooling in the *schleier* mutant fin tip (H) compared with wild-type fin tip (G).

mutant, we were able to recover recombinant fish that had fin overgrowth and retained only the C583Y mutation.

Slc12a7a is predicted to encode a potassium chloride co-transporter Kcc4a. Given our previous finding that *kcnk5b*, a potassium channel, is involved in regulating proportion and has an overgrowth phenotype similar to *schleier*, *slc12a7a* was a strong candidate. We identified a single unique missense mutation in the *slc12a7a* gene, C583Y, present in all *schleier* mutants and absent in wild-type siblings (0/56) (Fig. 3A). Kcc4a protein that contains the C583Y mutation is likely not functional, as the mutation eliminates a cysteine residue predicted to form a critical disulfide bond (DiANNA analysis (Ferre and Clote, 2005);).

To test whether mutations in *slc12a7a/kcc4a* could result in fin overgrowth, we designed specific guide RNAs (gRNAs) targeted against the third exon of the gene that should affect all predicted isoforms of Kcc4a. These guides were injected with Cas9 mRNA into wild-type embryos. Strikingly, adults from injected embryos (P0) showed broad proportional overgrowth of fins and barbels (Fig. 3B). Additionally, similar to homozygous *schleier* mutants, an alteration of pigmentation stripe pattern was seen in the anal and caudal fins (Fig. 3B). The observed phenotypes were localized to specific areas of the fin and likely due to mosaicism in injected animals. Overgrown areas of fins revealed elongation of fin ray segments similar to that seen in *schleier* (Fig. 3C). Genotypic analysis of the overgrown fin tissue showed deletions in exon 3 of *slc12a7a/kcc4a* at high percentage (12/16; 75%; Fig. 3D). The majority of the mutations detected (11/12; 92%) were predicted to cause a frameshift in the translated protein resulting in a premature stop codon shortly thereafter.

Zebrafish have two *slc12a7/kcc4* paralogues that share 74% amino acid identity. Using *in situ* hybridization (ISH), we detected *slc12a7a/kcc4a* transcript at modest levels in wildtype intra-ray and inter-ray fin mesenchyme and epidermis (Fig. 4A). *Schleier* heterozygous caudal fin tissue had similar levels of expression but a slightly more punctate expression pattern (Fig. 4B). Quantitative PCR analysis did not detect any difference in *slc12a7a/kcc4a* transcript levels between wild-type and *schleier* heterozygous fin tissue (Fig. 4C). We also performed *in situ* hybridization to detect the expression pattern of the paralogue *slc12a7b/kcc4b*. This transcript was detected faintly in wild-type fin mesenchyme and epidermis with scattered darkly staining, punctate regions (Fig. 4D). While no obvious difference in ISH staining pattern for *slc12a7b/kcc4b* was observed between wild-type and *schleier* fin tissue (Fig. 4E), qPCR measurement determined that *schleier* heterozygous fins had significantly decreased expression of the paralogue transcript (Fig. 4F).

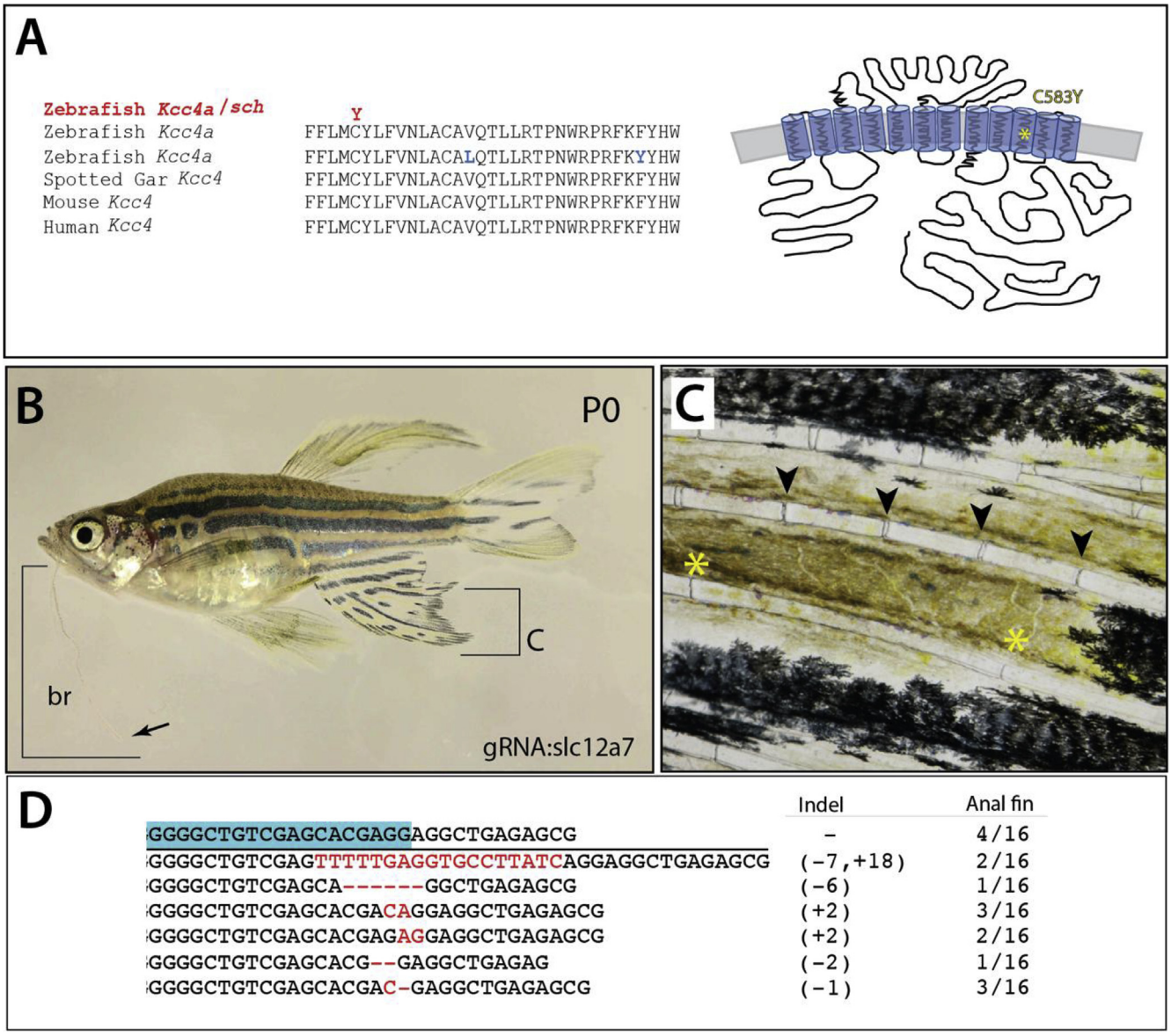

Fig. 3. ***Schleier* is caused by mutation of *slc12a7a* encoding potassium chloride cotransporter Kcc4a. A)** Multispecies alignment of predicted coding sequence of *slc12a7a* showing position of altered residue in Kcc4a in the *schleier* mutant. Schematic representation redrawn after (Marcoux et al., 2017). **B**) Adult wildtype P0 zebrafish with somatic clones harboring deletions of *slc12a7a/kcc4a*. Arrow points to tip of barbel; bracket shows extent of growth. **C**) Close up of anal fin labeled in (B) showing elongated segments of the rays (joints marked *); normal segmentation pattern observed just above (arrowheads). **D**) Sequence of deletions identified in affected region of anal fin and frequency (12/16); blue box, sequence of the guide RNA used in targeting.

Using antibodies against Kcc4 paralogues, we detected a single band of expected size when used on a Western blot of zebrafish tissue extracts (data not shown). As the target antigen is present in both Kcc4a and Kcc4b proteins, the antibody is predicted to recognize both paralogues in the zebrafish. The expression pattern of the Kcc4a/b proteins in fin cryosections showed Kcc4a/b protein expression in a pattern consistent with the *in situ* hybridization results described above. Kcc4a/b were detected in wild-type epidermis and mesenchyme with heightened punctate expression in specific cells or regions (Fig. 4G). In *schleier* fin mesenchyme and epidermis, immunofluorescence revealed decreased amount of Kcc4a/b protein as compared to wild-type fin, consistent with the qPCR data (Fig. 4J).

In order to quantitate and compare the number of *slc12a7a/kcc4a* and *slc12a7b/kcc4b* transcripts in wild-type fish, we used a publicly available database (www.zfregeneration.org (Nieto-Arellano and Sanchez-Iranzo, 2019);) to access RNAseq data of zebrafish fins. RNAseq analyses of wild-type, nonregenerative adult zebrafish caudal fins indicate that the absolute expression levels of both genes is low, at 5–15 FPKM (Fig. 4M and N); for comparison, *actinb1* transcripts are present at over 2000 FPKM in both data sets. These data also indicate that *slc12a7b/kcc4b* transcripts were detected approximately twice as often as *slc12a7a/kcc4a*. To confirm that the RNAseq data were relevant to fish from our own laboratory, we performed end-point PCR on cDNA from wild-type and *schleier* heterozygous caudal fin tissue. Our qualitative results were concordant with the above conclusions (Fig. 4O).

2.4. *Schleier C583Y mutation causes transporter loss-of-function*

Our previous work on the *kcnk5b/alf* long-finned mutant established that the *alf* mutation caused increased potassium transport. As the Kcc4a protein also mediates potassium transport, and the *schleier* mutant has strong phenotypic similarity to the *alf* mutant, our *a priori* expectation was that the *schleier* mutation would also cause increased protein activity. However, our gene targeting of *slc12a7a/kcc4a* indicated that loss-of-

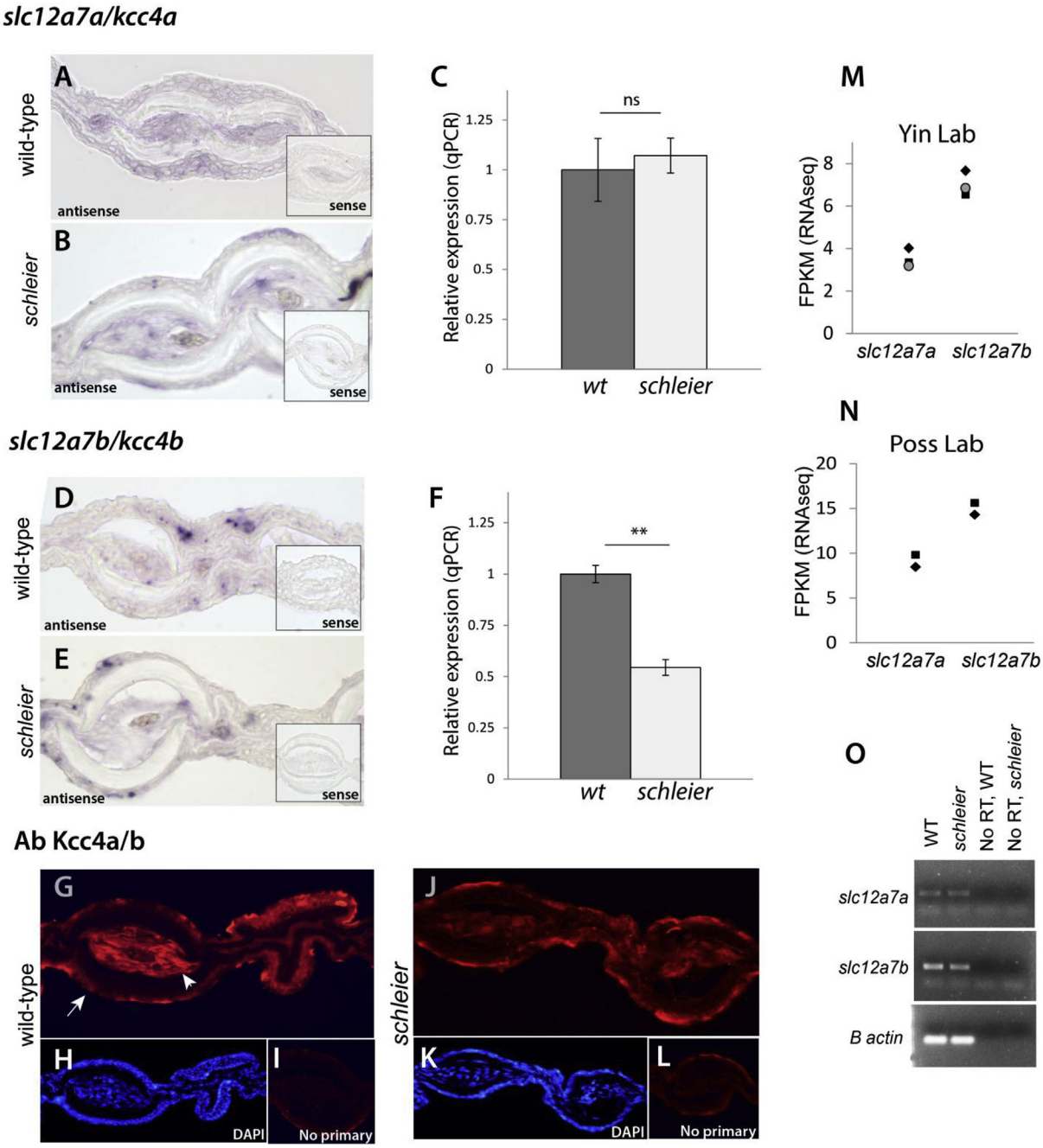

Fig. 4. Expression of *slc12a7a/kcc4a* and its paralog *slc12a7b/kcc4b* in fin mesenchyme. A, B) *In situ* hybridization of *slc12a7a/kcc4a* in cross sections of adult caudal fins of wild-type (A) and heterozygous *schleier* mutants (B). *Inset*, signal from control *in situ* probes on serial sections. C) Quantitative PCR measurement of *slc12a7a/kcc4a* transcript in wild-type and heterozygous *schleier* caudal fin tissue. Gene expression was normalized to the geometric mean of three reference genes; n = 4 samples per genotype; 4 adult fins per sample. Error bars indicate SEM; ns, not significant using Student's t-test. **C, D)** *In situ* hybridization of the paralogue *slc12a7b/kcc4b* in cross sections of adult caudal fins of wild-type (D) and heterozygous *schleier* mutants (E). *Inset*, signal from control *in situ* probes on serial sections. **F**) Quantitative PCR measurement of *slc12a7b/kcc4b* transcript in wild-type and heterozygous *schleier* caudal fin tissue. Gene expression was normalized to the geometric mean of three reference genes; n = 4 samples per genotype; 4 adult fins per sample. Error bars indicate SEM; *, $p < 0.01$ using Student's t-test. **G-L)**, Immunofluorescence of antibodies against Kcc4 in adult caudal fins. **G, J)** Experimental (primary plus secondary antibody) on wild-type and heterozygous *schleier* fin sections. Arrow, fin epidermis; arrowhead, fin mesenchyme. **H, K),** DAPI counterstaining of wild-type and heterozygous *schleier* fin sections. **I, L**) Signal from control sections hybridized with secondary antibody only. **M, N)** Number of *slc12a7a/kcc4a* and *slc12a7b/kcc4b* transcripts in wild-type caudal fin, measured in fragments per kilobase of transcript per million mapped reads (FPKM). Data were obtained from www.zfregeneration.org (Nieto-Arellano and Sanchez-Iranzo, 2019). O) Endpoint RT-PCR on cDNA synthesized from wild-type (WT) and *schleier* heterozygous caudal fin RNA. No RT, no reverse transcriptase control.

function mutations in the gene were sufficient to confer a long-finned phenotype. Given this unexpected result, we decided to determine the effect of the *schleier* C583Y mutation on the transporter activity of the Kcc4a protein.

cRNAs encoding wild-type or Kcc4a C583Y mutant protein were injected singly or as a mixture into *Xenopus laevis* oocytes under hypotonic conditions. Notably, the presence of the C583Y mutation resulted in a 90% decrease in transport activity (WT, 11686.7 ± 1555.3 vs C583Y, 968.1 ± 392.7 pmol/oocyte/h, $p < 0.001$; Fig. 5A), without modifying the total protein expression (Fig. 5A, **inset**). When co-expressed with C583Y, wild-type co-transporter function was significantly affected at the higher protein concentration tested (WT, 10110.1 ± 1256.3 vs WT:C583Y (0.2 μg/μl), 6785.5 ± 729.3 pmol/oocyte/h, $p < 0.05$) (Fig. 5B). Based on these observations, we conclude that the C583Y mutation causes loss of ion transport function in the KCC4a protein.

2.5. In-frame deletions in the slc12a7a/kcc4a gene cause alterations in fin size

The effect of Crispr-Cas induced mutations in *slc12a7a/kcc4a* in wild-type fish showed that mosaic inactivation of the gene was sufficient to cause fin overgrowth. However, it remained unknown which particular mutant alleles were capable of causing this phenotype. To address this question, we crossed mosaic P0 fish to wild-type fish to establish individual lines of F1 progeny heterozygous for unique alleles of *slc12a7a/kcc4a.* The F1 progeny displayed a range of phenotypes, from phenotypically wild-type to fish with long fins and extended barbels (Fig. 6B). Genotyping of phenotypically wild-type F1 fish revealed that some of these fish were heterozygous for deletions predicted to cause premature stop codons in exon 3 (Fig. 6A). Upon translation, such mutations would produce a truncated Kcc4a protein that was 99 amino acids in length, as compared to the 1117 amino acid wild-type protein; such a protein is probably nonfunctional and/or unstable. Based on the normal fin and barbel phenotypes observed in fish heterozygous for truncation alleles, we concluded that 50% reduction in Kcc4a protein was not sufficient to cause fin and barbel overgrowth. Subsequent crosses revealed that fish homozygous for the truncation allele are viable and phenotypically normal; thus, the *slc12a7a/kcc4a* gene is not essential for survival (data not shown).

We genotyped long-finned F1 fish to identify mutations that caused fin overgrowth and found that these fish were heterozygous for small in-frame deletions or insertions in exon 3 (Fig. 6A). Two such alleles were isolated from multiple independent founders. One allele contained a three amino acid deletion and caused only mild phenotypic changes such as long barbels (Fig. 6C). A second allele caused a six amino acid deletion that resulted in significantly elongated barbels and long fins; this mutant also exhibited disrupted stripe pattern in the anal fin (Fig. 6B and C). These phenotypes were similar to those seen in the *schleier* mutant but with decreased severity. The deletions occur in the N-terminal domain of the protein, predicted to be cytoplasmic (Fig. 6D). Interestingly, the size of the deletion correlated with the degree of the overgrowth phenotype (Fig. 6E) suggesting that Kcc4a is quite sensitive to the presence of nonfunctional variants.

We assessed whether fish with in-frame deletions in *slc12a7a/kcc4a* exhibited changes in vascular tone similar to those observed with *schleier* heterozygous fish by performing high speed videomicroscopy on fish with the six amino acid in-frame deletion allele. Analysis of these fish showed alterations in vein:artery diameter (1.07 ± 0.08; mean ± SEM) and relative vein:artery velocity (0.38 ± 0.05; mean ± SEM) distinct from wild type values (vein:artery diameter, 1.50 ± 0.12; vein:artery velocity, 0.52 ± 0.02; mean ± SEM) (Supplementary Fig. 3). Interestingly, these values were also significantly different from *schleier*, suggesting dynamic vascular patterning is associated with these mutants (Supplementary Fig. 3).

2.6. Epistasis of potassium channel signaling mediating reveals common pathway of growth regulation

We have previously demonstrated that activating mutations in the potassium channel *kcnk5b* caused patterned overgrowth of fins and barbels, and that absence of *kcnk5b* had no effect on fin phenotype (Daane et al., 2018; Perathoner et al., 2014). Given the similarity between the *kcc4a* and *kcnk5b* overgrowth phenotypes, we hypothesized that they might work in a similar pathway or act in parallel to regulate

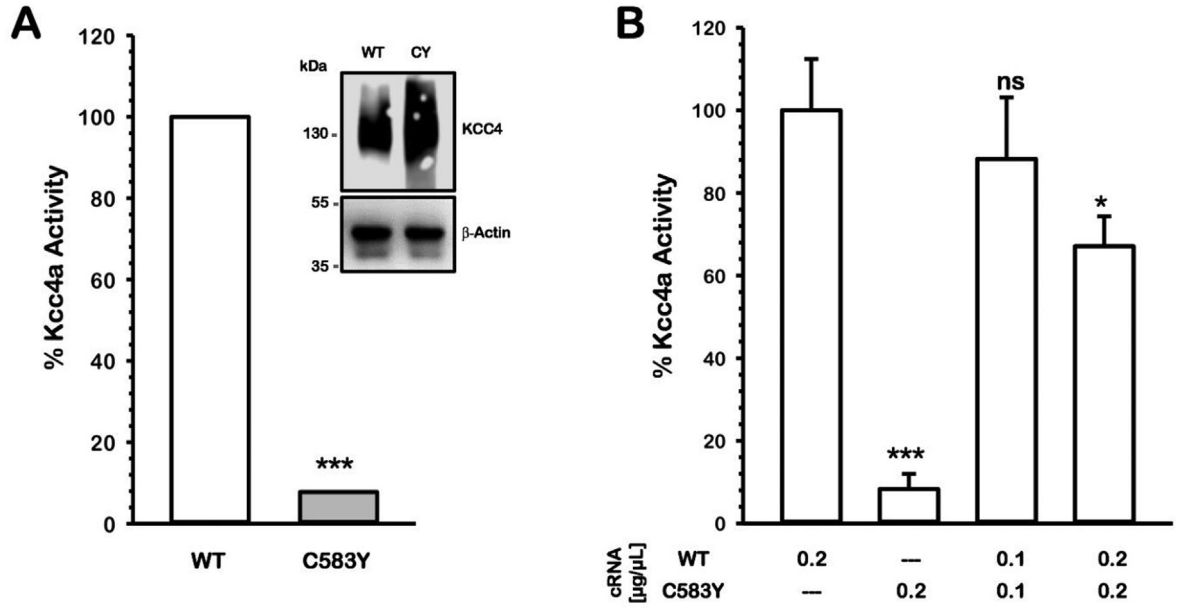

Fig. 5. The effect of the C583Y mutation results in disruption of co-transport function of Kcc4a. A) Percentage of activity was determined as the Cl^--dependent, Rb^+ cotransport by Slc12a7a/Kcc4a tested in *Xenopus* oocytes through expression of wild-type (WT) and C583Y Kcc4a under hypotonic conditions. *Inset* shows protein expression from total extracts. **B)** Percentage of Kcc4a activity co-expressed with different concentrations of C583Y mutant as shown. For both **A** and **B**, mean ± SEM are shown. n.s., not significant; *$p < 0.05$; ***$p < 0.0001$ calculated using a student's T test in comparison to wildtype Kcc4a. Results presented are the summed activity of three separate experiments; n = 30 oocytes per group.

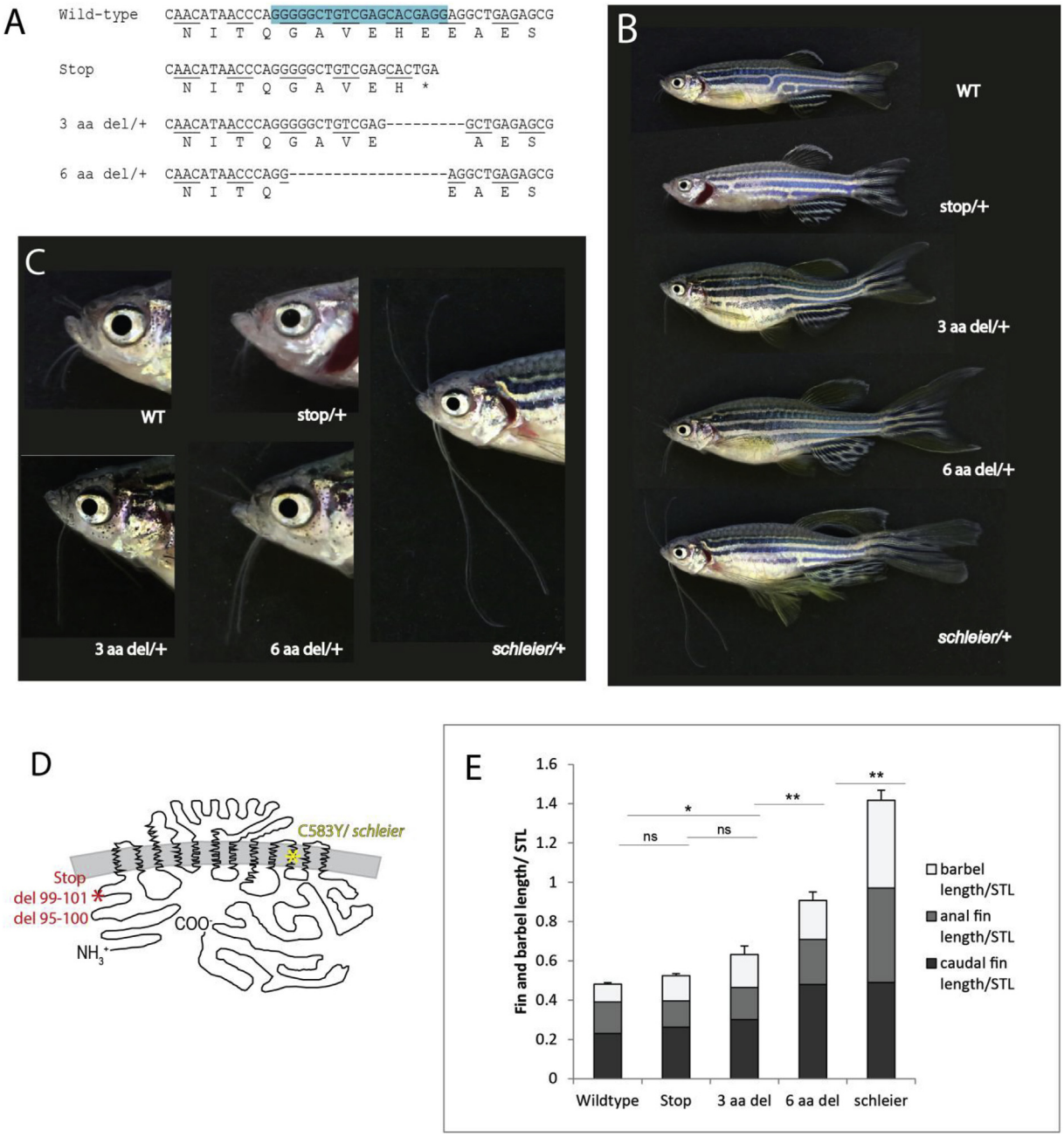

Fig. 6. Allelic titration of *slc12a7a/kcc4a* expressivity revealing necessity and sensitivity to levels of Kcc4a during development. A) Identified deletions in F1 progeny and predicted protein alteration; blue box, sequence targeted by guide RNA. **B)** Representative pictures of individuals heterozygous for different *slc12a7a/kcc4a* alleles. **C)** Barbel phenotypes conferred by different *slc12a7a/kcc4a* alleles. **D)** Schematic of Kcc4a protein depicting locations of premature stop codon, 3 amino acid deletion, 6 amino acid deletion (red asterisk), and *schleier* mutation (yellow asterisk). **E)** Tabulation of relative length of fins and barbels in F1 progeny heterozygous for each genotype; mean ± SEM is shown. n.s., not significant; *$p < 0.05$; **$p < 0.01$ calculated using a one-way ANOVA followed by a Tukey's multiple comparisons test; n = 6–19 fish per genotype.

growth.

We decided to test for interaction between the *slc12a7a/kcc4a* and *kcnk5b* genes. We designed two guide RNAs to target exon 1 of *kcnk5b* and co-injected them into *schleier* heterozygous embryos and their wild-type siblings. Injected P0 fish were grown to maturity, genotyped, and assessed for their fin and barbel phenotypes. Clonal analysis on anal fin tissue verified that the guide RNAs successfully introduced deletions and/or insertions at the targeted sites (Fig. 7D). As would be expected based on our earlier work (Perathoner et al., 2014), (Daane et al., 2018), targeted inactivation of *kcnk5b* had no effect in a wild-type genetic background (Fig. 7A). However, CRISPR-mediated inactivation of *kcnk5b* in a heterozygous *slc12a7a/schleier* background produced fish with reduced anal fin and barbel length (Fig. 7C). Barbel length was nearly restored to wild-type, while anal fin length was significantly shorter than in *slc12a7a* heterozygotes (Fig. 7E, G). The average length of individual anal fin ray segments was also shorter in *slc12a7a* +/-; *gkcnk5b* fish, and the shape of the caudal fin was narrower and less billowy than the veil-like *schleier* mutant phenotype (Fig. 7F, C). Unlike the regional overgrowth caused by upregulation of *kcnk5b*, the phenotype of *slc12a7a/kcc4a* +/-; *gkcnk5b* fish appeared to be systemic in nature, affecting whole structures and exhibiting consistent phenotypes in all fish.

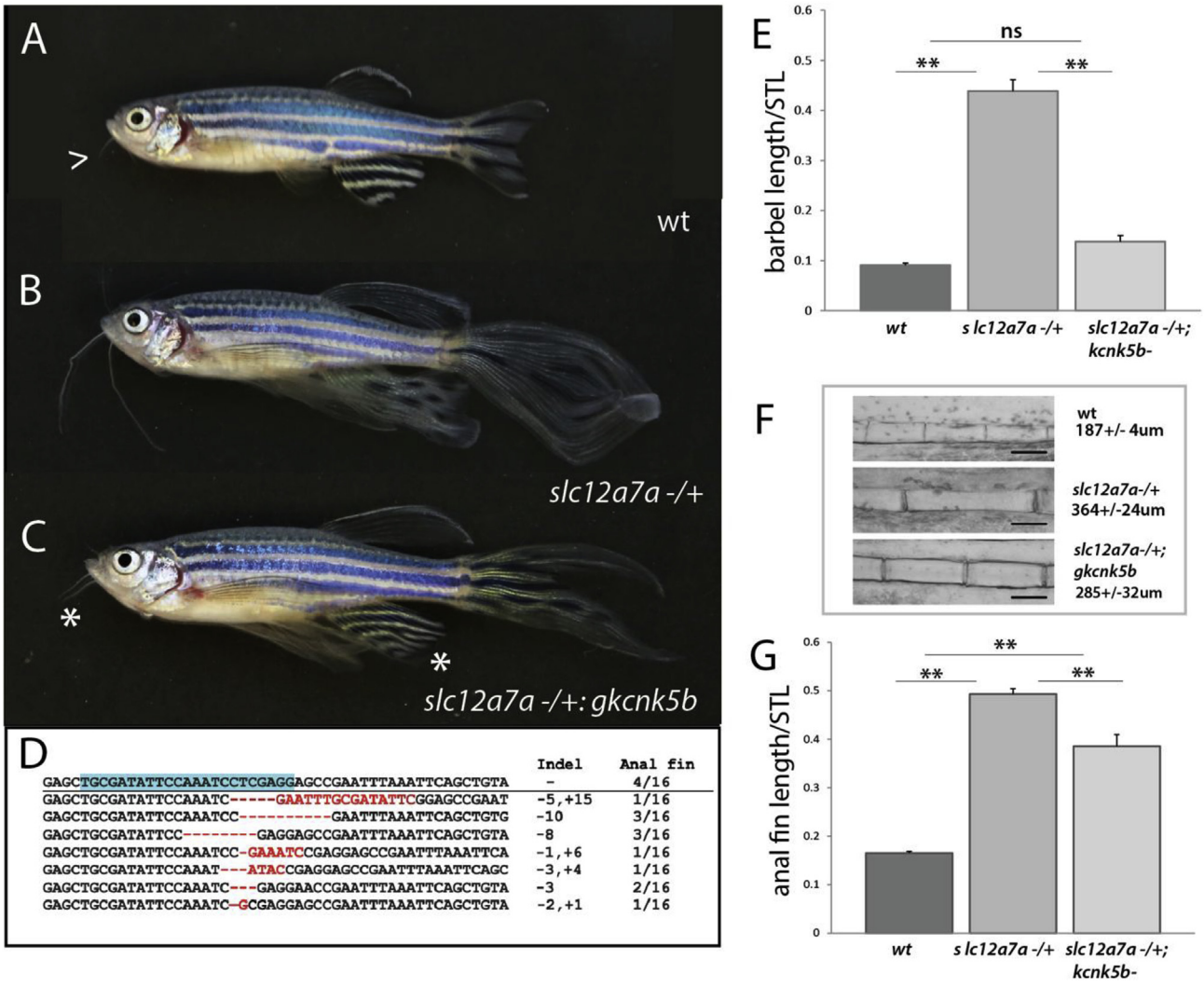

Fig. 7. Regulation of size in *schleier* requires functional *kcnk5b*. A-C) Representative pictures of growth phenotypes of zebrafish with altered potassium channel function. A) Wild-type adult zebrafish; arrowhead, end of barbel. **B**) *schleier* heterozygote. **C**) *schleier* heterozygote fish harboring somatic deletion clones within *kcnk5b*, (*gkcnk5b*); asterisk demarcates reduction of overgrowth phenotype of the barbel and anal fins. **D**) Deletions detected in *kcnk5b* from reverted anal fins in affected mutants. Blue highlight = targeted sequence. **E-G**) Reversion of *schleier* overgrowth phenotypes after abrogation of *kcnk5b* function. **E**) Barbel length relative to standard length (STL). **F**) Size of segments within anal fin rays. **G**) Anal fin length relative to STL. For **E-G**, mean ± SEM is shown for each panel. n.s., not significant; **p < 0.01 calculated using a one-way ANOVA with a Tukey's multiple comparisons test; n = 7–24 fish per genotype.

3. Discussion

3.1. Role for Kcc4a in bioelectric signaling

Research into bioelectric signaling has seen a recent boom, revealing essential roles of electrochemical fields and ion channel activity during development and regeneration (McLaughlin and Levin, 2018). Importantly, many of these functions can be attributed to non-excitable tissues with changes reflected in consistent shifts of resting membrane potential of cells and across tissues. Genetic models of ion channel mutations often have very specific neurological or physiological phenotypes. Of the channels discussed in this work, both Kcnk5b (TASK2) and Kcc4 knockout mice have kidney defects due to alteration in ionic regulation in the thick ascending arm of the kidney (Barriere et al., 2003; Warth et al., 2004). Kcc4 KO mice additionally have hearing defects (Boettger et al., 2002). However, neither of the mouse knockouts provides insight into the potential role of ion channels in growth and patterning, and it remains unclear whether bioelectric signaling plays a consistent role in these processes. Clinical presentations of ion channelopathies retain this bias towards phenotypes caused by changes in excitable cell populations such as muscle, nerve or endocrine tissue (Felix, 2000).

The Kcnj2/Kir2.1 protein provides one of the rare examples in which changes in channel function lead to patterning defects and dysmorphologies (Dahal et al., 2012, 2017). Analysis of Kcnj2 in *Xenopus* has shown that modification of resting membrane potential across early ectoderm can alter craniofacial development, consistent with the spectrum of clinical phenotypes caused by mutations in this channel (Adams et al., 2016; Donaldson et al., 2004). Zebrafish mutants provide other prominent examples that begin to illuminate the extent of potassium channel regulation in growth and development, such as Kcnj13 in patterning pigment stripes (Iwashita et al., 2006) and Kcnk5b in regulating fin size regulation (Perathoner et al., 2014). These mutants are for the most part gain-of-function and thus can be considered supra-physiological cases not resembling 'normal' mechanisms of development. Here, we describe a functional role for *slc12a7a/kcc4a* in regulating size and growth of the zebrafish fin through diminishing the fraction of functional channels (Supplementary Fig. 4). These data support the essential nature of bioelectric signaling in the regulation and development of proportion.

3.2. Genetic basis of Kcc4a function in size regulation

Kcc4 has two paralogues in zebrafish, *kcc4a* and *kcc4b*. Our expression data suggest that the two paralogues and their encoded isoforms have overlapping patterns of expression in fin mesenchyme and epidermis. Surprisingly, presence of the *schleier* C583Y mutation in *slc12a7a/kcc4a* resulted in decreased expression of *slc12a7b/kcc4b* transcript as determined by qPCR and decreased Kcc4a/b protein in the fin mesenchyme and epidermis. It is unclear what the underlying mechanism is for this decrease.

Our data identify that the *schleier* mutation in *slc12a7a/kcc4a* causes a loss of size regulation at the phenotypic level and a loss of transport function at the protein level. However, fish heterozygous or homozygous for a premature stop mutation in *slc12a7a/kcc4a* have normal fin size (Fig. 6 and data not shown); thus, the mutation is neither haploinsufficient nor essential. We propose that the *schleier* mutation has a dominant negative effect on the Kcc4a protein. Given that the protein functions as a membrane bound dimer (Bergeron et al., 2011), mutations such as *schleier* that result in the formation of full-length, though inactive, protein should cause a greater decrease in the levels of functional Kcc4a dimer than loss of one allele (Supplementary Fig. 4). Consistent with this, we observed that heterozygosity for in-frame deletions and the *schleier* C583Y mutation, but not heterozygosity for a null mutation, resulted in fin and barbel overgrowth. Interestingly, the phenotypic effects of Kcc4a gain-of-function mutations are scaled to the size of the in-frame deletions and can be titrated (Fig. 6).

The Kcc4 protein has been shown to form heterodimers with other KCC and NKCC family members via their C-terminal domains (Simard et al., 2007). Our data support an interpretation in which the dominant negative effect of Kcc4a variants is exerted in part through formation of heterodimers with the paralogue Kcc4b. Consistent with this notion, our data indicate that the *slc12a7a/kcc4a* and *slc12a7b/kcc4b* transcripts have overlapping expression patterns. Formation of heterodimers *in vivo* might buffer against fluctuations in potassium transport caused by loss of one or more alleles. It would be of interest to investigate whether inactivation of the paralogue *slc12a7b/kcc4b* or of other *kcc/nkcc* family members increases the severity of the observed phenotype and reveals a fundamental requirement for potassium regulation during normal development.

3.3. Dose dependent functions and threshold responses

The *schleier* mutation in *slc12a7a/kcc4a* causes a dominant increase in the relative proportion of the fins and barbs as well as a recessive pigment phenotype affecting patterning of the adult stripes. Among zebrafish with mutations affecting conductivity, *schleier* is the first mutant to share both fin and pigment phenotypes. These pleiotropic effects may reflect the extent to which the mutated Kcc4a channel oligomerizes with other KCC or NKCC channels to inhibit or modify their function (Simard et al., 2007). Interestingly, the *schleier* pigment phenotype closely resembles the phenotype of fish with mutations in *cx41.8* (Irion et al., 2014; Watanabe et al., 2006) but not those with mutations in *kcnj13* (Iwashita et al., 2006). Thus, Kcc4a may be tied to the regulation of bioelectric signaling through Cx41.8 mediated cell connectivity in pigment patterning and through Cx43 in development of fin length (Iovine et al., 2005; Perathoner et al., 2014). The presence of the pigment phenotype in homozygous *kcc4a/schleier* mutants but not heterozygotes could reflect differential sensitivity of growth versus pigment pathways to changes in *Vmem*, or alternatively, could reflect a dominant negative effect of the *schleier* mutation on other signaling processes and other channels.

How bioelectric signals are transduced into a growth response in the fin, and their specificity, remains an open area of investigation. Changes in membrane polarization may alter influx and balance of critical intracellular signaling ions like calcium, resulting in changes to the transcriptional program and cell proliferation. Alternatively, or in addition to this, changes to the overall ion concentration in a tissue environment may directly alter the properties of local cells and tissues. Our data indicate that *slc12a7a/kcc4a* and its paralogue *slc12a7b/kcc4b* have similar expression patterns in fin mesenchyme and epidermis. The distinct punctate expression pattern of the *slc12a7b/kcc4b* transcript and the Kcc4a/b protein may reflect discrete subpopulations of mesenchymal cells, such as dermis or osteoblasts. However, the identity of these cells and their role during fin development remains to be discerned.

Given the critical role of potassium as a regulator of vascular tone, the vasculature is a tissue likely to be impacted by loss of Kcc4a function. The presence of mutant Kcc4a in fin mesenchyme might impair potassium transport and cause increased potassium in extracellular fluid adjacent to the fin blood vessels, resulting in vasoconstriction of the arteries. In support of this, we observed that fins with *slc12a7a/kcc4a* mutations had increased blood flow to the fin tip. This blood pooling at the distal margin of the fin is accompanied by persistence of a capillary nexus and is present in both *slc12a7a/kcc4a* and *kcnk5b* long-finned mutants. The increased arterial blood flow was accompanied by slower return transit through fin veins, which were grossly enlarged to accommodate the larger volume (Supplementary Movie 2). These anatomical changes could prolong exposure to circulating growth factors; thus, ion-mediated changes in vascular tone might provide one means via which these mutations affect growth.

3.4. Genetic epistasis among potassium channels and regulation of coordinated growth and size

Our data suggest that potassium homeostasis within cells and across tissues may be a key regulator of size in the zebrafish fin. In previous work, we demonstrated that gain-of-function mutations in the potassium channel protein Kcnk5b result in fin and barbel overgrowth. Here, we show that mutations in Kcc4a, another protein involved in potassium transport, produce a similar long-finned phenotype. The phenotypes of *schl/kcc4a* and *alf/kcnk5b* closely resemble each other, suggesting they may regulate similar pathways. The expression pattern of Kcc4a in the fin mesenchyme is similar to the tissue we have shown is responsible for Kcnk5b growth regulation in transplants (Perathoner et al., 2014); thus, these factors are likely operating in the same cells. Our findings further suggest that the Kcc4a and Kcnk5b proteins work in concert, and that alterations in the function of either component can increase growth. The *kcnk5b* long-finned mutations cause increased potassium transport, while the *schleier* mutation causes a loss-of-transport function. Although deletion of *kcnk5b* fails to have a growth phenotype, we have previously shown that the function of this channel was necessary for enhanced growth caused by FK506-mediated inhibition of calcineurin (Daane et al., 2018). Here, we show that *kcnk5b* is also required for the effect of the *schleier* mutation in Kcc4a. Whether this genetic relationship is additive or epistatic remains an open question. We find that unlike overexpression of *kcnk5b* or loss of *slc12a7a/kcc4a,* which act in a local manner in the fin causing outgrowth, loss of *kcnk5b* seems to affect size regulation of the fins overall, suggesting a potential systemic role in suppression of growth. As both channels are expressed in the kidney and play roles in regulating hypertension, this may be a facet of regulation for further investigation.

3.5. Core components of growth regulation mediated by integration of potassium channel function

The alteration in the net flow of ions within a tissue will have a direct effect on the resting membrane potential of a cell, *Vmem*. Consistent with this fact, we have shown that gain-of-function mutations in Kcnk5b lead to hyperpolarization of *Xenopus* oocytes (Perathoner et al., 2014). We favor an additive hypothesis for regulation of growth signals by potassium channel regulation, with the effects of each gene summated in the resting membrane potential of a cell (Fig. 8A). In this model, channels such as Kcc4a and Kcnk5b integrate environmental stimuli as well as systemic regulators of growth into classic signaling pathways in tissues, coordinating diverse signals into a bioelectric response (Bagriantsev et al., 2011; Daane et al., 2018; McClenaghan et al., 2016). We propose that multiple inputs affect potassium ion concentration and contribute to

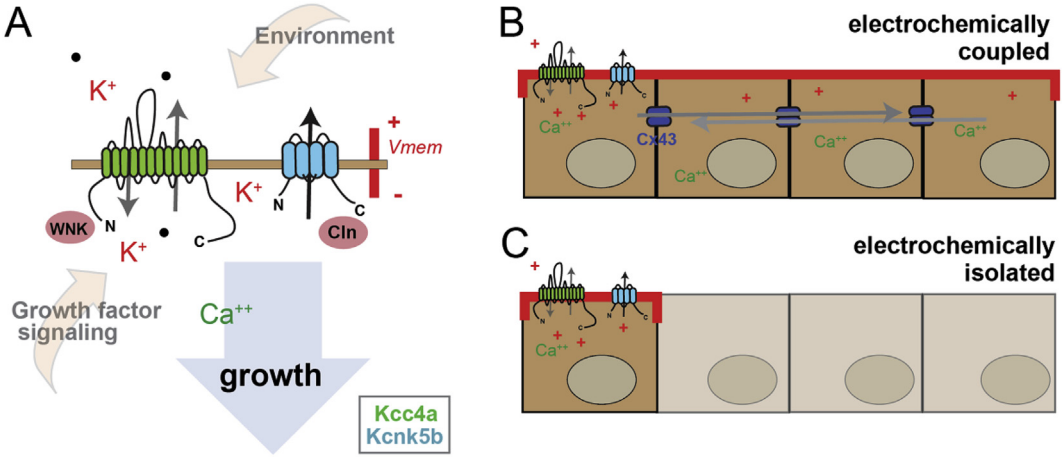

Fig. 8. Model of bioelectrical signal integration during growth of the zebrafish fin. Multifaceted integration of environmental and classical secondary signal messengers in regulating resting membrane voltage by potassium channel activity. **A**) Regulation of ionic conductance across a plasma membrane through additive inputs of Kcc4a and Kcnk5b channel regulation. Kcc4 is electroneutral, transporting K+ and Cl- (•) ions across membrane; at normal resting potential, K+ flux is normally outwards. The action of KCC channels can be regulated by cytoplasmic factors such as WNK kinases allowing integration with other signaling pathways. Kcnk5b is an outward leak channel gated in part through environmental conditions such as pH, as well as internal signaling factors binding to the C-terminus. Calcineurin (Cln) is a key signaling factor that links Kcnk5b function to canonical signaling pathways (Daane et al., 2018). We suggest that the combined output of Kcc4a and Kcnk5b alters resting membrane potential, and that this ionic modulation may serve as a broader readout of environmental changes and of levels of intracellular secondary messengers resulting from growth factor signaling. As Kcnk5b is necessary for expression of growth effects of Kcc4a and calcineurin inhibition, we posit that it acts as translator of changes in membrane potential to calcineurin-mediated growth. **B–C**) Model of electrocoupling of cells and potential for coordinated growth in development. **B**) A shift in membrane resting potential can have effects that extend across cells and thus coordinate potentially noisy developmental signals. This regulation is mediated in the developing and regenerating fin by gap junctions comprised of Cx43. This electrocoupling leads to non-cell-autonomous effects in growth as seen in loss of *slc12a7a/kcc4a* or *kcnk5b* expression. **C**) Lack of cell electrocoupling; signals would be predicted to be restricted and less coordinated.

a common bioelectrical signaling response in the zebrafish fin. This system is sensitive even to slight alterations in protein function, as seen in the *slc12a7a/kcc4a* CRISPR alleles. Classical growth factors may also provide input to this network, such as Igf1, an important paracrine regulator of relative proportion that acts in part to control coordinated growth within tissues (Yakar et al., 2018). Notably, Igf1 has been found to upregulate Kcc3 and Kcc4 activity in cancer cells, suggesting it can mediate activity of this proposed network (Hsu et al., 2007; Shen et al., 2001). The potassium channel *kcnk5b* may play a core role in modulating the output of variations in *Vmem*, as it is needed for overgrowth in multiple contexts (Kcc4 inactivation, calcineurin inhibition (Daane et al., 2018)) and can itself lead to overgrowth when locally overexpressed or activated (Perathoner et al., 2014).

In this bioelectric signaling model, we would predict that membrane polarity is interpreted through steady state alterations in net *Vmem* within tissues (Fig. 8). Each potassium channel type will have specialized functions and will modify *Vmem* with different sensitivities to changes in local ionic potential as well as secondary signaling capabilities. Some channels may provide different phenotypic effects depending on their biological context. For example, our data demonstrate that loss of Kcc4 activity results in increased growth of the fin; however, clinical data indicate that increased Kcc4 activity correlates with invasiveness in human cancer cells (Brown et al., 2018; Chen et al., 2009; Zhou et al., 2018). These seemingly conflicting observations lend support to the concept that alterations in resting *Vmem* are key to regulating growth and coordinated cell interactions in tissues during development and homeostasis (Levin, 2014). In the context of the zebrafish fin, our model predicts that decreasing the potassium gradient across mesenchymal and epidermal cells leads to hyperpolarization of resting membrane potential and promotes growth (Fig. 8A). Manifestation of this growth response within cells of the developing fin also requires intracellular communication through gap junctions (Fig. 8B and C) (Iovine, 2005; Perathoner et al., 2014). An extension of this model is that reduction or elimination of this connectivity may underlie the loss of coordinated growth in neoplastic tissues (Litan and Langhans, 2015; Lobikin et al., 2012).

4. Conclusion remarks

Here we find that potassium channel function and bioelectric signaling are necessary for the normal establishment of proportion and size in development. We posit a model in which growth of the fin is modulated by relative changes in *Vmem*. This signal is translated into growth in part through the action of Kcnk5b, which may act as a central rheostat to modulate calcium-dependent growth (Daane et al., 2018). Application of this bioelectric model to understanding neoplastic growth and migration is pertinent given that many tumor types exhibit increased expression of potassium channels from diverse protein families and with different conductive and gating properties (Lang and Stournaras, 2014; Prevarskaya et al., 2010; Wang, 2004). Further analysis of regulators of this genetic pathway may reveal the checks and balances of tissue formation, homeostasis, and how coordination of growth is regulated during development and regeneration.

5. Materials and methods

5.1. Husbandry

All fish strains used were housed and maintained as described in (Nusslein-Volhard and Dahm, 2002) and performed in accordance with IACUC guidelines at Boston Children's Hospital and Wheaton College. A complete description of the husbandry and environmental conditions in housing for the fish used in these experiments at Boston Children's Hospital is available as a collection in protocols.io (https://doi.org/10.17504/protocols.io.mrjc54n). Similar conditions were present at Wheaton College. For all experiments, adult stages were defined by reproductively mature fish >3 months old. Males and females were used together in analyses as both sexes showed comparable changes in growth regulation.

5.2. Photography and measurement of fish, fins, barbels, and fin segments

Fish were anesthetized in MS-222 prior to photography. Whole fish

photographs were taken using a Canon EOS 6D camera with a Canon 500D 77 mm close-up lens. Photographs were analyzed using Fiji (Schindelin et al., 2012) to obtain standard length (STL) determined as the length from the tip of the snout to the posterior end of the caudal peduncle; caudal and anal fin length, determined as the length of the longest fin ray; fin area; and barbel length. For fin segment analysis, fins of anesthetized fish were photographed using a Nikon SMZ800 dissecting microscope and a Spot Insight 2 camera with Spot software. Fin and barbel length were normalized for each fish by dividing by standard length. ANOVA was used to compare mean fin and/or barbel length/STL among different genotypes of fish. Fin segment lengths were measured using Fiji; a minimum of 20 segments were measured per fish. Segment length data from a minimum of 4 fish were used to calculate mean and SEM.

5.3. Mutagenesis, modifier screen, identification, and genotyping of schleier

Homozygous *longfin* (dt2) mutant males were mutagenized with 3.3 μM N ethyl-n-nitrosourea for four repeated doses following (Rohner et al., 2011). Founder mutagenized males were crossed to Tubingen wildtype females. F1 progeny were scored for reduction or increase of heterozygous *longfin* phenotype. An enhancer mutant was identified that led to an increase in length of all fins and barbs in the heterozygous *lof* background. This mutant was outcrossed and isolated as an independent locus affecting fin growth. The mutant was named *schleier* and given the allele assignment *dmh39*. The mutation underlying the *schleier* mutant phenotype was identified through whole genome sequencing and mapped through identity by descent as previously outlined (Bowen et al., 2012). The C583Y variant was identified in *slc12a7a* on chromosome 2 and was found to be tightly linked to the *schleier* phenotype.

Genotyping the C583Y *slc12a7a/kcc4a* mutation was carried out as follows: DNA was extracted from fin clips using the NaOH method of Meeker et al. DNA was denatured at 95 °C and snap cooled on ice, then used as template for PCR amplification using PrimeSTAR DNA polymerase (Takara) under manufacturer conditions. Genotyping primers are as follows: F: 5′-GTACAGGTTTTTCTTGATGT-3′, R: 5′-GAAAGGCTCAGGCTCATCCC-3′. PCR products were Sanger sequenced using the reverse primer.

5.4. Creation of slc12a7a/kcc4a and kcnk5b knockouts

For *slc12a7a*, the online tool ZiFit was used to design guides to target exon 3 of isoform 002 of *D. rerio slc12a7a*. This exon is shared by all 3 major splice isoforms of the gene. The target sequence 5′-GGGGGCTGTCGAGCACGAGG-3′ was used for designing primers TAGGGGGCTGTCGAGCACGAGG and AAACCCTCGTGCTCGACAGCCC which were synthesized, annealed and placed into the BsaI-digested vector pDR274 (Addgene) using the method of Hwang et al. *Slc12a7a* guide RNA was synthesized from this vector using the MEGAshortscript T7 Kit (Ambion) as per manufacturer's instructions.

For *kcnk5b*, the online tool CHOPCHOP was used to design two guides to target exon 1 of *D. rerio kcnk5b*. The two target sequences were 5′-TGCGATATTCCAAATCCTCGAGG-3′ and 5′-ATATCCCTGCCTAAGTAAAGAGG-3′. Guide RNAs (crRNA) for the target sequences and tracrRNA were synthesized by Integrated DNA Technologies. RNAs were resuspended in nuclease-free H_20 at 100 μM concentration. The crRNA and tracrRNA were then annealed in manufacturer-provided duplex buffer by heating to 95 °C and cooling to room temperature at 20 μM concentration.

Guide RNAs were mixed with Cas9 SmartNuclease eukaryotic mRNA (System Biosciences) such that the final concentration of RNA was approximately 350 ng/uL for each gene (150 ng/ul guide RNA, 300 ng/ul Cas9 RNA). This mixture was injected into single-cell *D. rerio* wild-type (AB) embryos or *schleier*/+ embryos, depending on the experiment. After two days, DNA from individual embryos was extracted using the NaOH method of Meeker et al. and analyzed by PCR and Sanger sequencing. Exon 3 of *slc12a7a* was PCR amplified using the primers F: 5′-GCCGTAAATAAGGTG-3′, R: 5′-CTGTGTGGGAGTCTAGTTG-3′. Exon 1 of *kcnk5b* was PCR amplified using the primers F: 5′-AGAAACTTGGGAGTGTGGAGTG-3′, R: 5′-TTCCCAAAACACAAATGAAACA-3′; this primer pair will detect mutations introduced by either *kcnk5b* guide. PCR products were subcloned into pGEM-T and individual clones were sequenced to determine whether mutations had been introduced at the targeted sequence.

Injected fish (P0) were grown to maturity and used for fin length analyses. *Slc12a7a*-injected P0 fish were subsequently crossed to wild-type AB fish to generate F1 progeny with unique mutations. When DNA analysis was required, anesthetized fish were subjected to fin clip, and DNA extraction and subsequent analysis was carried out on fin tissue as above to identify mutations.

5.5. Construction of Slc12a7a/Kcc4a expression vector

Full length *D. rerio slc12a7a/kcc4a* was PCR amplified from cDNA of wildtype fin and subcloned in pGEM-T (F: 5′-GCACTTTTGTCTCCGTGTCAGC-3′, R: 5′-CATCTTGCTGGAACAGAAACTGAGG-3′). Copy cutter cells (Epicentre) were used for propagation as the *slc12a7a/kcc4a* gene product was toxic to commonly used bacteria when at high copy number. The *slc12a7a/kcc4a* cDNA was subcloned into the *Xenopus* expression vector pXT7 (Addgene). Subsequently, the C583Y mutation was introduced into the *slc12a7a/kcc4a* pXT7 construct using a QuikChange II Kit (Agilent) as per the manufacturer's protocol.

5.6. Assessment of the K+:Cl-cotransporter function and immunoblot

K+:Cl-cotransport activity of wild-type Kcc4a and its mutant C583Y was assessed using the heterologous expression system of *Xenopus laevis* oocytes following our standard procedures (Adragna et al., 2015; Kahle et al., 2005; Melo et al., 2013). Briefly, mature oocytes were injected with water alone or containing 0.2 μg/μl of Kcc4a cRNA alone or together with its mutant C583Y. Two days after injection, the activity of K+:Cl-cotransport was determined by measuring the Cl–dependent 86Rb + uptake under hypotonic conditions (~110 mOsm). All transport assays were performed with groups of 10–15 oocytes pre-incubated for 30 min at room temperature in a Na+ and Cl-free medium (in mM: 50 N-methyl-D-glucamine- gluconate, 10 K + -gluconate, 4.6 Ca2+-gluconate, 1 Mg + -gluconate, and 5 HEPES/Tris, pH 7.4) and then transferred to the uptake medium (in mM: 40 N-methyl-D-glucamine-Cl−, 10 KCl, 1.8 CaCl2, 1 MgCl2, and 5 HEPES/Tris, pH 7.4) containing 0.5 μCi of 86Rb+/ml for 1 h at 32 °C. Tracer activity was determined for each oocyte by β-scintillation counting.

For the immunoblot, total extracts of two oocyte equivalents injected with WT or C583Y cRNA were obtained using ice-cold lysis buffer (in mM: 50 Tris-HCl (pH 7.5), 1 EGTA, 1 EDTA, 50 NaF, 5 Na4O7P2, 1 Na3VO4, 1% (w/v) Nonidet P40, 0.27 sucrose, 0.1% 2-mercaptoethanol) supplemented with a protease inhibitor cocktail (1 tablet per 50 ml, Sigma). Total KCC4 antibody used was previously described (Adragna et al., 2015; Kahle et al., 2005; Melo et al., 2013), while β-actin and secondary antibody coupled to horseradish peroxidase used were obtained from Santa Cruz.

5.7. Analysis of vascular flow

To compare flow rate and diameter of vessels, three fish of each genotype were analyzed (mass = 0.48 ± 0.02 g; STL = 26 ± 0.5 mm; +/- = SEM). Each fish was lightly anesthetized by submersion in a dilute concentration of 0.04% MS-222; 0.01 ml of 0.005 mg/ml pancuronium bromide (Sigma) was then injected intraperitoneally for immobilization (Arnaout et al., 2007), as even minor movements caused video artifacts. Fish were then transferred to an MS-222 soaked sponge with a small cutout; this set-up stabilized the fish while allowing for the maintenance of anesthesia and a moist environment. Each fish was kept in this setup

for a maximum of 10 min. Heart rate was recorded before and after data collection to verify that the experimental procedure did not alter heart rate. Throughout the experiment, diluted anesthetic was repeatedly introduced over the gills to ensure the fish remained anesthetized and well-ventilated. For data collection, the fish was moved to the stage of a Nikon Eclipse E400 microscope which was fitted with a HiSpec Lite camera to record at 200 fps with a resolution of 704 × 528 pixels. The fish was filmed at the posterior-most tip of the caudal fin under 200× magnification. Fish were euthanized by MS-222 overdose immediately following video recording.

Supplementary video related to this article can be found at https://doi.org/10.1016/j.ydbio.2019.08.016.

From the video data, blood vessel diameter and red blood cell velocity were measured using ImageJ software (Rueden et al., 2017). Blood vessel diameter was measured near the tip of the caudal fin for the major artery running through the second-most dorsal fin ray and from the paired vein directly above it. The diameter of each vessel was measured in at least five positions and data were pooled per individual fish. From these measurements, a ratio of vein:artery diameter for each fish was calculated and compared among different genotypes using an ANOVA. Red blood cell velocity was similarly measured at the tip of the caudal fin artery and vein. For each vessel, a minimum of ten red blood cells were tracked for 10–50 frames (50–250 ms) each by using the MTrackJ plugin https://imagescience.org/meijering/software/mtrackj/. Data were pooled within individual fish for each velocity location. As was performed for the diameter analysis, a ratio of vein:artery red blood cell velocity was calculated per fish and compared between among different genotypes of fish using an ANOVA.

5.8. Immunofluorescence and in situ hybridization

Caudal fins were amputated using a razor blade from adult fish anesthetized with 0.04% MS-222. Fins were fixed for 1 h at room temperature and then at 4 °C overnight in a solution of 4% paraformaldehyde/PBS, pH 7.4. After overnight fixation, 0.5 M EDTA solution was added to the sample for a final concentration of 0.25 M EDTA and incubated for an additional 24 h at 4 °C. Fins were rinsed several times in PBS and moved gradually through a sucrose/PBS solutions of increasing sucrose concentration (15 % × 2 hours, 20 % × 2 hours, 30% overnight) while kept at 4 °C. The following day, fins were transferred to cryo-embedding medium (Tissue-Tek O.C.T compound) in cryomolds and allowed to equilibrate for at least 1 h at room temperature. Samples were then flash frozen in isopentane chilled in a dry ice-isopentane bath, and transferred to -80 °C. For cryosectioning, blocks were allowed to warm to –20 °C, then sectioned into 10 μM transverse sections using a Microm HM 505N microtome cryostat. Sections were collected onto Fisherbrand ColorFrost Plus slides, dried for 1 h at 37 °C, dried overnight at room temperature, and then stored at -80 °C for up to 3 months.

Immunofluorescence: Slides were thawed at room temperature. After drying slightly, an ImmunoPen (Sigma) was used to isolate individual sections. Sections were incubated in blocking solution (5% goat serum in PBS) in a humidified chamber for 1 h at room temperature. After block was removed, primary antibody (KCC4/SLC12A7 rabbit polyclonal antibody, Novus Biologicals NBP1-49583) was added at 1:100 dilution in PBST (1% goat serum, 0.3% Tween in PBS). Slides were incubated in primary antibody in a humidified chamber overnight at 4 °C. Slides were washed gently in PBST and then incubated in secondary antibody at 1:200 dilution (Goat anti-Rabbit IgG (H + L) Secondary Antibody, Alexa Fluor® 555 conjugate, ThermoFisher) in PBST for 1 h at room temperature in a dark humidified chamber. Slides were washed gently in PBST, mounted in Prolong Diamond antifade mount with DAPI (ThermoFisher) and glass coverslips, and dried overnight at room temperature in the dark. Slides were imaged using a Nikon Eclipse E400 microscope equipped for fluorescence detection and photographed with a Spot Insight 2 Camera.

In situ hybridization: Slides were thawed at room temperature, then post-fixed in 4% paraformaldehyde/PBS, pH 9.5 for 1 h at room temperature. Following fixation, slides were rinsed thoroughly in PBS in Coplin jars, dehydrated in an ethanol series (70%, 95%, 100%) and allowed dry at room temperature before permeabilization with 1% Triton X-100 in PBS (20 min, room temperature). Slides were rinsed again in PBS and dehydrated in ethanol as above. Slide edges were sealed with an ImmunoPen.

Hybridization procedures were modified from (Smith et al., 2008). Probes were diluted 1:150 in hybridization buffer (1X salt [0.2 M NaCl, 10 mM Tris HCl, 5 mM NaH_2PO_4, 5 mM Na_2HPO_4, 1 mM Tris base, 5 mM EDTA], 50% deionized formamide, 10% dextran sulphate, 0.05 mg/ml yeast tRNA, and 1× Denhardts). Probes were heated for 10 min at 70 °C, then placed on ice briefly before applying to slides. Slides with probe were incubated flat in RNAse-free containers humidified with 1X salt/50% formamide at 55 °C for 48 h. After incubation, slides were washed in solution A (1× SSC, 50% formamide, and 0.1% Tween 20) three times at 55 °C (15 min, 30 min, 30 min), then washed twice in MABT (100 mM maleic acid, 150 mM NaCl, 0.1% Tween-20, pH 7.5) at room temperature for 30 min per wash). Slides were placed flat in containers humidified with dH_20 and incubated in a small volume of blocking solution (20% heat-inactivated sheep serum in MABT) overnight at 4 °C. Block solution was removed and anti-digoxigenin-AP, Fab fragments (Sigma) diluted 1:2000 in fresh blocking solution was added. Slides were incubated in antibody for a minimum of 24 h at 4 °C. Slides were then washed at room temperature as follows: 4 washes of 20 min each in MABT, followed by 2 washes of 10 min each in NTMT staining buffer (100 mM NaCl, 100 mM Tris HCL pH 9.5, 50 mM MgCl2, and 1% Tween 20). Slides were placed flat in containers humidified with dH_20 and incubated in BM Purple (Sigma) in the dark at room temperature for 48 h. After development of signal, slides were washed in PBS-0.1% Triton and fixed in 4% PFA/PBS overnight at 4 °C. Slides were washed in ddH_20, allowed to dry briefly, and mounted in CC mount (Sigma) under glass coverslips. After overnight drying, slides were photographed using a Nikon Eclipse E400 microscope with a Spot Insight 2 Camera.

5.9. In situ probe cloning and synthesis

Primer3 was used to design PCR primers in exons 21 and 26 of the primary transcript of the *slc12a7a/kcc4a gene* (F: 5′-GATGGAACAACGCTCACAGA-3′; R: 5′-GAGGACCTCCAGAAACTCCA-3′) and in exons 23 and the 3′ UTR of the primary transcript of the *slc12a7b/kcc4b* gene (F: 5′-ATGCCTGGACCACCGAAAAA-3′; R: 5′- ATCAAGCGACAAGCCGATGA-3′). These primers were used to amplify a 517 or 572 base pair PCR product, respectively, from caudal fin cDNA, which was then subcloned into the pGEM-T vector using TA cloning. For probe generation, 10 μg of purified plasmid was digested with SacI or SacII restriction enzyme, phenol-chloroform extracted, precipitated with sodium acetate/ethanol, and resuspended in nuclease-free H_20. 1 μg purified digested plasmid was used as template for SP6 or T7 transcription using the DIG-RNA labeling kit (Roche). Following probe transcription, DNA template was removed using Turbo DNAse kit (In Vitrogen). Probe was precipitated by incubation in 0.1 M LiCl, 75% ethanol overnight at –80 °C, followed by centrifugation and wash in 70% ethanol. After drying slightly, probe pellet was resuspended in 50% nuclease-free H_20/50% formamide and stored at –80 °C. An aliquot of probe was analyzed using agarose electrophoresis to verify probes were expected sizes and not degraded.

5.10. cDNA preparation, qPCR, and endpoint PCR

Wild-type or *schleier* heterozygous caudal fins were collected in pools of four adult fins per sample, minimum of four samples per genotype. Fins were homogenized in Trizol (Ambion); total RNA was subsequently extracted according to manufacturer's instructions and stored at -80 °C. RNA quantity and quality was assessed using a Qubit fluorometer

(ThermoFisher). 1 μg RNA aliquots from each sample were subjected to DNAse treatment using TURBO DNA-free kit (ThermoFisher), then used as templates for reverse transcription with the AMV First Strand cDNA synthesis kit and oligo-dT primer (New England Biolabs). The resulting cDNA was diluted in nuclease-free water and used as template for qPCR.

qPCR experiments were designed, executed, and analyzed using methodologies described in (Taylor et al., 2019). Experiments were performed using an AriaMx real-time PCR system and Brilliant III Ultra-Fast SYBR Green qPCR Master Mix according to the manufacturer's suggested protocols (Agilent). Primer sequences are listed in Supplementary Table 1. Standard curves were generated for each primer set to assess efficiency; all primers had efficiencies between 1.9-2.1. Gene sequences for *slc12a7a* and *slc12a7b* were downloaded from Ensembl, and gene-specific primers were designed using Primer-Blast (National Center for Biotechnology Information). Following PCR amplification, PCR products were subjected to a melting curve and agarose gel electrophoresis to verify the presence of a single amplicon. Relative *slc12a7a* or *slc12a7b* levels in wild-type and *schleier* heterozygous fish were normalized to the geometric mean of the three reference genes (*eef1a1l1, actb,* and *tuba1b)*. Data were analyzed using the comparative Ct (ΔΔCt) method. Results represent the mean of four biological replicates.

For qPCR normalization, potential reference genes and primers were selected based on prior analyses of adult zebrafish tissue (McCurley and Callard, 2008; Sopezki et al., 2018) and then tested for their stability in wild-type and *schleier* fin tissue. Using the online tool RefFinder (Xie et al., 2012), the genes *eef1a1l1, actb,* and *tuba1b* were identified as stably expressed among fin tissue samples and were used for normalization.

Endpoint PCR was performed using *slc12a7a, slc12a7b,* and *actb* primers (Supplementary Table 1), cDNAs prepared as described above, and GoTaq Master Mix (Promega). Amplification was done in a PTC-100 cycler (MJ Research) for 30 s each at 95 °C, 55 °C, 72 °C, for a total of 35 cycles. PCR products were visualized on a 2% agarose gel using SYBR-safe dye (ThermoFisher).

Acknowledgements

The authors would like to thank prior work by Simon Perathoner, Iris Koch, and Ines Gehring on the *schleier* mutant and its isolation. JL thanks Amanda Bettle and Beth Amaral for fish husbandry.

Appendix A. Supplementary data

Supplementary data to this article can be found online at https://doi.org/10.1016/j.ydbio.2019.08.016.

Funding

This work was partially supported by funding by the National Institutes of Health [R01HD084985 to MPH; 1 R01NS109358-0 to KK], the Simons Foundation, March of Dimes, and the Hydrocephalus Association. The funding agencies had no input on the study design nor presentation of the data within.

Author contributions

JL, KK, and MPH designed experimental strategy in this work; JL, KK, DP, LE, HC, CS, MB, AM, GG performed experiments supporting the data presented. JL and MPH wrote first and JL, KK, and MPH were involved with subsequent drafts and revisions of the paper.

Conflicts of interest

The authors have no competing interests regarding the data presented in this work.

References

Adams, D.S., Uzel, S.G., Akagi, J., Wlodkowic, D., Andreeva, V., Yelick, P.C., Devitt-Lee, A., Pare, J.F., Levin, M., 2016. Bioelectric signalling via potassium channels: a mechanism for craniofacial dysmorphogenesis in KCNJ2-associated Andersen-Tawil syndrome. J. Physiol. 594, 3245–3270.

Adragna, N.C., Ravilla, N.B., Lauf, P.K., Begum, G., Khanna, A.R., Sun, D., Kahle, K.T., 2015. Regulated phosphorylation of the K-Cl cotransporter KCC3 is a molecular switch of intracellular potassium content and cell volume homeostasis. Front. Cell. Neurosci. 9, 255.

Arnaout, R., Ferrer, T., Huisken, J., Spitzer, K., Stainier, D.Y., Tristani-Firouzi, M., Chi, N.C., 2007. Zebrafish model for human long QT syndrome. Proc. Natl. Acad. Sci. U. S. A. 104, 11316–11321.

Bagriantsev, S.N., Peyronnet, R., Clark, K.A., Honore, E., Minor Jr., D.L., 2011. Multiple modalities converge on a common gate to control K2P channel function. EMBO J. 30, 3594–3606.

Barriere, H., Belfodil, R., Rubera, I., Tauc, M., Lesage, F., Poujeol, C., Guy, N., Barhanin, J., Poujeol, P., 2003. Role of TASK2 potassium channels regarding volume regulation in primary cultures of mouse proximal tubules. J. Gen. Physiol. 122, 177–190.

Bergeron, M.J., Boggavarapu, R., Meury, M., Ucurum, Z., Caron, L., Isenring, P., Hediger, M.A., Fotiadis, D., 2011. Frog oocytes to unveil the structure and supramolecular organization of human transport proteins. PLoS One 6, e21901.

Boettger, T., Hubner, C.A., Maier, H., Rust, M.B., Beck, F.X., Jentsch, T.J., 2002. Deafness and renal tubular acidosis in mice lacking the K-Cl co-transporter Kcc4. Nature 416, 874–878.

Bowen, M.E., Henke, K., Siegfried, K.R., Warman, M.L., Harris, M.P., 2012. Efficient mapping and cloning of mutations in zebrafish by low-coverage whole-genome sequencing. Genetics 190, 1017–1024.

Brown, T.C., Murtha, T.D., Rubinstein, J.C., Korah, R., Carling, T., 2018. SLC12A7 alters adrenocortical carcinoma cell adhesion properties to promote an aggressive invasive behavior. Cell Commun. Signal. 16, 27.

Chen, Y.F., Chou, C.Y., Wilkins, R.J., Ellory, J.C., Mount, D.B., Shen, M.R., 2009. Motor protein-dependent membrane trafficking of KCl cotransporter-4 is important for cancer cell invasion. Cancer Res. 69, 8585–8593.

Daane, J.M., Lanni, J., Rothenberg, I., Seebohm, G., Higdon, C.W., Johnson, S.L., Harris, M.P., 2018. Bioelectric-calcineurin signaling module regulates allometric growth and size of the zebrafish fin. Sci. Rep. 8, 10391.

Dahal, G.R., Pradhan, S.J., Bates, E.A., 2017. Inwardly rectifying potassium channels influence Drosophila wing morphogenesis by regulating Dpp release. Development 144, 2771–2783.

Dahal, G.R., Rawson, J., Gassaway, B., Kwok, B., Tong, Y., Ptacek, L.J., Bates, E., 2012. An inwardly rectifying K+ channel is required for patterning. Development 139, 3653–3664.

Donaldson, M.R., Yoon, G., Fu, Y.H., Ptacek, L.J., 2004. Andersen-Tawil syndrome: a model of clinical variability, pleiotropy, and genetic heterogeneity. Ann. Med. 36 (Suppl. 1), 92–97.

Felix, R., 2000. Channelopathies: ion channel defects linked to heritable clinical disorders. J. Med. Genet. 37, 729–740.

Ferre, F., Clote, P., 2005. DiANNA: a web server for disulfide connectivity prediction. Nucleic Acids Res. 33, W230–W232.

Gokhale, R.H., Shingleton, A.W., 2015. Size control: the developmental physiology of body and organ size regulation. Wiley Interdiscip. Rev. Dev. Biol. 4, 335–356.

Hoptak-Solga, A.D., Klein, K.A., DeRosa, A.M., White, T.W., Iovine, M.K., 2007. Zebrafish short fin mutations in connexin43 lead to aberrant gap junctional intercellular communication. FEBS Lett. 581, 3297–3302.

Hsu, Y.M., Chou, C.Y., Chen, H.H., Lee, W.Y., Chen, Y.F., Lin, P.W., Alper, S.L., Ellory, J.C., Shen, M.R., 2007. IGF-1 upregulates electroneutral K-Cl cotransporter KCC3 and KCC4 which are differentially required for breast cancer cell proliferation and invasiveness. J. Cell. Physiol. 210, 626–636.

Huxley, J., 1932. Problems in Relative Growth. The Dial Press.

Huxley, J., Teissier, G., 1936. Terminology of relative growth. Nature 137, 780–781.

Inaba, M., Yamanaka, H., Kondo, S., 2012. Pigment pattern formation by contact-dependent depolarization. Science 335, 677.

Iovine, M.K., Higgins, E.P., Hindes, A., Coblitz, B., Johnson, S.L., 2005. Mutations in connexin43 (GJA1) perturb bone growth in zebrafish fins. Dev. Biol. 278, 208–219.

Irion, U., Frohnhofer, H.G., Krauss, J., Colak Champollion, T., Maischein, H.M., Geiger-Rudolph, S., Weiler, C., Nusslein-Volhard, C., 2014. Gap junctions composed of connexins 41.8 and 39.4 are essential for colour pattern formation in zebrafish. Elife 3, e05125.

Iwashita, M., Watanabe, M., Ishii, M., Chen, T., Johnson, S.L., Kurachi, Y., Okada, N., Kondo, S., 2006. Pigment pattern in jaguar/obelix zebrafish is caused by a Kir7.1 mutation: implications for the regulation of melanosome movement. PLoS Genet. 2, e197.

Kahle, K.T., Rinehart, J., de Los Heros, P., Louvi, A., Meade, P., Vazquez, N., Hebert, S.C., Gamba, G., Gimenez, I., Lifton, R.P., 2005. WNK3 modulates transport of Cl- in and out of cells: implications for control of cell volume and neuronal excitability. Proc. Natl. Acad. Sci. U. S. A. 102, 16783–16788.

Lang, F., Stournaras, C., 2014. Ion channels in cancer: future perspectives and clinical potential. Philos. Trans. R. Soc. Lond. B Biol. Sci. 369, 20130108.

Lawson, N.D., Weinstein, B.M., 2002. In vivo imaging of embryonic vascular development using transgenic zebrafish. Dev. Biol. 248, 307–318.

Levin, M., 2014. Endogenous bioelectrical networks store non-genetic patterning information during development and regeneration. J. Physiol. 592, 2295–2305.

Levin, M., Pezzulo, G., Finkelstein, J.M., 2017. Endogenous bioelectric signaling networks: exploiting voltage gradients for control of growth and form. Annu. Rev. Biomed. Eng. 19, 353–387.
Litan, A., Langhans, S.A., 2015. Cancer as a channelopathy: ion channels and pumps in tumor development and progression. Front. Cell. Neurosci. 9, 86.
Lobikin, M., Chernet, B., Lobo, D., Levin, M., 2012. Resting potential, oncogene-induced tumorigenesis, and metastasis: the bioelectric basis of cancer in vivo. Phys. Biol. 9, 065002.
Marcoux, A.A., Garneau, A.P., Frenette-Cotton, R., Slimani, S., Mac-Way, F., Isenring, P., 2017. Molecular features and physiological roles of K(+)-Cl(-) cotransporter 4 (KCC4). Biochim. Biophys. Acta Gen. Subj. 1861, 3154–3166.
McClenaghan, C., Schewe, M., Aryal, P., Carpenter, E.P., Baukrowitz, T., Tucker, S.J., 2016. Polymodal activation of the TREK-2 K2P channel produces structurally distinct open states. J. Gen. Physiol. 147, 497–505.
McCurley, A.T., Callard, G.V., 2008. Characterization of housekeeping genes in zebrafish: male-female differences and effects of tissue type, developmental stage and chemical treatment. BMC Mol. Biol. 9, 102.
McLaughlin, K.A., Levin, M., 2018. Bioelectric signaling in regeneration: mechanisms of ionic controls of growth and form. Dev. Biol. 433, 177–189.
Melo, Z., de los Heros, P., Cruz-Rangel, S., Vazquez, N., Bobadilla, N.A., Pasantes-Morales, H., Alessi, D.R., Mercado, A., Gamba, G., 2013. N-terminal serine dephosphorylation is required for KCC3 cotransporter full activation by cell swelling. J. Biol. Chem. 288, 31468–31476.
Misu, A., Yamanaka, H., Aramaki, T., Kondo, S., Skerrett, I.M., Iovine, M.K., Watanabe, M., 2016. Two different functions of Connexin43 confer two different bone phenotypes in zebrafish. J. Biol. Chem. 291, 12601–12611.
Nieto-Arellano, R., Sanchez-Iranzo, H., 2019. zfRegeneration: a database for gene expression profiling during regeneration. Bioinformatics 35, 703–705.
Nusslein-Volhard, C., Dahm, R., 2002. Zebrafish: a Practical Approach. Oxford University Press, Oxford.
Othmer, H.G., Pate, E., 1980. Scale-invariance in reaction-diffusion models of spatial pattern formation. Proc. Natl. Acad. Sci. U. S. A. 77, 4180–4184.
Perathoner, S., Daane, J.M., Henrion, U., Seebohm, G., Higdon, C.W., Johnson, S.L., Nusslein-Volhard, C., Harris, M.P., 2014. Bioelectric signaling regulates size in zebrafish fins. PLoS Genet. 10, e1004080.
Prevarskaya, N., Skryma, R., Shuba, Y., 2010. Ion channels and the hallmarks of cancer. Trends Mol. Med. 16, 107–121.
Rohner, N., Perathoner, S., Frohnhofer, H.G., Harris, M.P., 2011. Enhancing the efficiency of N-ethyl-N-nitrosourea-induced mutagenesis in the zebrafish. Zebrafish 8, 119–123.
Rueden, C.T., Schindelin, J., Hiner, M.C., DeZonia, B.E., Walter, A.E., Arena, E.T., Eliceiri, K.W., 2017. ImageJ2: ImageJ for the next generation of scientific image data. BMC Bioinf. 18, 529.
Schindelin, J., Arganda-Carreras, I., Frise, E., Kaynig, V., Longair, M., Pietzsch, T., Preibisch, S., Rueden, C., Saalfeld, S., Schmid, B., Tinevez, J.Y., White, D.J., Hartenstein, V., Eliceiri, K., Tomancak, P., Cardona, A., 2012. Fiji: an open-source platform for biological-image analysis. Nat. Methods 9, 676–682.
Shen, M.R., Chou, C.Y., Hsu, K.F., Liu, H.S., Dunham, P.B., Holtzman, E.J., Ellory, J.C., 2001. The KCl cotransporter isoform KCC3 can play an important role in cell growth regulation. Proc. Natl. Acad. Sci. U. S. A. 98, 14714–14719.
Simard, C.F., Bergeron, M.J., Frenette-Cotton, R., Carpentier, G.A., Pelchat, M.E., Caron, L., Isenring, P., 2007. Homooligomeric and heterooligomeric associations between K+-Cl- cotransporter isoforms and between K+-Cl- and Na+-K+-Cl- cotransporters. J. Biol. Chem. 282, 18083–18093.
Smith, A., Zhang, J., Guay, D., Quint, E., Johnson, A., Akimenko, M.A., 2008. Gene expression analysis on sections of zebrafish regenerating fins reveals limitations in the whole-mount in situ hybridization method. Dev. Dynam. 237, 417–425.
Sopezki, M.D.S., Monserrat, J.M., Yunes, J.S., Zanette, J., 2018. Validation of housekeeping genes as internal controls for the study of the effects of microcystin-LR in zebrafish by real-time PCR. Zebrafish 15, 454–459.
Taylor, S.C., Nadeau, K., Abbasi, M., Lachance, C., Nguyen, M., Fenrich, J., 2019. The ultimate qPCR experiment: producing publication quality, reproducible data the first time. Trends Biotechnol. 37, 761–774.
Umulis, D.M., Othmer, H.G., 2013. Mechanisms of scaling in pattern formation. Development 140, 4830–4843.
Vollmer, J., Casares, F., Iber, D., 2017. Growth and size control during development. Open Biol. 7.
Wang, Z., 2004. Roles of K+ channels in regulating tumour cell proliferation and apoptosis. Pflüg. Arch. 448, 274–286.
Warth, R., Barriere, H., Meneton, P., Bloch, M., Thomas, J., Tauc, M., Heitzmann, D., Romeo, E., Verrey, F., Mengual, R., Guy, N., Bendahhou, S., Lesage, F., Poujeol, P., Barhanin, J., 2004. Proximal renal tubular acidosis in TASK2 K+ channel-deficient mice reveals a mechanism for stabilizing bicarbonate transport. Proc. Natl. Acad. Sci. U. S. A. 101, 8215–8220.
Watanabe, M., Iwashita, M., Ishii, M., Kurachi, Y., Kawakami, A., Kondo, S., Okada, N., 2006. Spot pattern of leopard Danio is caused by mutation in the zebrafish connexin41.8 gene. EMBO Rep. 7, 893–897.
Watt, K.I., Harvey, K.F., Gregorevic, P., 2017. Regulation of tissue growth by the mammalian hippo signaling pathway. Front. Physiol. 8, 942.
Xie, F., Xiao, P., Chen, D., Xu, L., Zhang, B., 2012. miRDeepFinder: a miRNA analysis tool for deep sequencing of plant small RNAs. Plant Mol. Biol. 80 (1), 75–84.
Yakar, S., Werner, H., Rosen, C.J., 2018. Insulin-like growth factors: actions on the skeleton. J. Mol. Endocrinol. 61, T115–T137.
Zhou, C., Feng, X., Yuan, F., Ji, J., Shi, M., Yu, Y., Zhu, Z., Zhang, J., 2018. Difference of molecular alterations in HER2-positive and HER2-negative gastric cancers by whole-genome sequencing analysis. Cancer Manag. Res. 10, 3945–3954.